Climate change key driver of catastrophic impacts of Hurricane Helene that devastated both coastal and inland communities

Authors

Ben Clarke, *Centre for Environmental Policy, Imperial College, London, UK*
Clair Barnes, *Centre for Environmental Policy, Imperial College, London, UK*
Nathan Sparks, *Department of Physics, Imperial College London, UK*
Ralf Toumi, *Grantham Institute - Climate Change and the Environment, Imperial College, London, UK*
Wenchang Yang, *Department of Geosciences, Princeton University, Princeton, NJ 08544, USA*
Joseph Giguere, *Climate Central, Princeton, NJ 08542, USA*
Bernadette Woods Placky, *Climate Central, Princeton, NJ 08542, USA*
Daniel Gilford, *Climate Central, Princeton, NJ 08542, USA*
Andrew Pershing, *Climate Central, Princeton, NJ 08542, USA*
Shel Winkley, *Climate Central, Princeton, NJ 08542, USA*
Gabriel A. Vecchi, *Department of Geosciences, Princeton University, Princeton, NJ 08544, USA; High Meadows Environmental Institute, Princeton University, Princeton, NJ, USA*
Julie Arrighi, *Global Disaster Preparedness Centre, American Red Cross, Washington D.C., USA; Red Cross Red Crescent Climate Centre, The Hague, The Netherlands; University of Twente, Enschede, The Netherlands (based in New York, USA)*
Malini Roy, *University of Arizona, Tuscon, USA*
Leah Poole-Selters, *Tufts University, Boston, USA*
Carolyn Van Sant, *Tufts University, Boston, USA*
Matthew Grieco, *American Red Cross, Washington D.C., USA*
Roop Singh, *Red Cross Red Crescent Climate Centre, The Hague, The Netherlands; Columbia University, New York, USA (based in New Jersey, USA)*
Maja Vahlberg, *Red Cross Red Crescent Climate Centre, The Hague, the Netherlands; Swedish Red Cross, Stockholm, Sweden (based in Ubmeje/Umeå, Sweden)*
Sarah Kew, *Royal Netherlands Meteorological Institute (KNMI), De Bilt, The Netherlands*
Izidine Pinto, *Royal Netherlands Meteorological Institute (KNMI), De Bilt, The Netherlands*
Friederike Otto, *Centre for Environmental Policy, Imperial College, London, UK*

Review authors

Victoria Hess, *American Red Cross, Washington D.C., USA*
Ellen Gorham, *American Red Cross, Washington D.C., USA*

Sam Rodgers, *American Red Cross, Washington D.C., USA*
Sjoukje Philip, *Royal Netherlands Meteorological Institute (KNMI), De Bilt, The Netherlands*
Joyce Kimutai, *Centre for Environmental Policy, Imperial College, London, UK*

Main findings

- Hurricane Helene formed in the Gulf of Mexico above record-hot sea surface temperatures (SSTs). In the days leading up to Helene's landfall, a line of slow-moving storms formed along a stalled cold front, drawing in tropical moisture from Helene's outer edges. This system, stretching from Atlanta through the southern Appalachian region, led to very heavy rainfall in the southern states and Appalachia even before the heavy rainfall associated with Helene arrived, leading to devastating flooding. Overall, at least 227 people died, the highest death toll from a hurricane in the mainland US since Katrina in 2005.
- In addition to the very heavy rainfall caused by the hurricane, and the preceding rain event, the steepness of the terrain funnelled rainwater into rivers and streams leading to extremely sudden flash flooding as high as rooftop levels making evacuations impossible in many regions.
- In today's climate, that has already been warmed by 1.3 °C due primarily to the burning of fossil fuels, weather observations indicate that rainfall events as severe as those brought by hurricane Helene now occur about once every 7 (3 – 25) years in the coastal region, and about once every 70 (20 – 3000) years in the inland region.
- To determine the role of climate change in the rainfall we combine observations with climate models. In both regions, the rainfall was about 10% heavier due to climate change, and equivalently the rainfall totals over the 2-day and 3-day maxima were made about 40% and 70% more likely by climate change, respectively. If the world continues to burn fossil fuels, causing global warming to reach 2 °C above pre industrial levels, devastating rainfall events in both regions will become another 15-25 % more likely.
- The IRIS model was used to investigate Helene's strong winds by analysing storms making landfall within 2 degrees of Helene. By statistically modelling storms in a 1.3°C cooler climate, this model showed that climate change was responsible for an increase of about 150% in the number of such storms (now once every 53 years on average, up from every 130 years), and equivalently that the maximum wind speeds of similar storms are now about 6.1 m/s (around 11%) more intense.
- The environmental conditions leading to a storm of Helene's intensity were also studied. Using the same approach as for rainfall, we find that climate change increased the potential intensity in September around the track of Helene increased strongly in likelihood by a factor of 18. Using the Ocean Climate Shift Index, we find that the sea surface temperatures (SSTs) over the track of the storm have been made about 200-500 times more likely due to the burning of fossil fuels.
- Together, these findings show that climate change is enhancing conditions conducive to the most powerful hurricanes like Helene, with more intense rainfall totals and wind speeds. This is in line with other scientific findings that Atlantic tropical cyclones are becoming wetter under climate change and undergoing more rapid intensification.
- Hurricane Helene was very well forecast with the national agency NOAA urging media to warn people of "catastrophic and life-threatening" flooding and landslides across the Southern Appalachians. People in affected coastal regions were asked to evacuate ahead of the landfall of Helene. However, most of the deaths occurred farther inland, in the mountainous terrain where challenges such as spotty cell and internet services, limited experience with Hurricanes and more limited evacuation infrastructure have been reported in the media as leaving people feeling caught off guard.

- Along the inland path of Hurricane Helene a network of dams, and drainage systems exists, that has long been identified as highly exposed to hazards and in a general state of disrepair. A catastrophic dam failure was ultimately avoided, despite evacuations downstream of at least 3 dams warning of potential failure. However, current flood protection infrastructure is not accounting for heavy rain cascading into landslides and mudslides in mountainous regions, as happened in the inland region leading to the destruction of homes, businesses and roads.

1 Introduction

Late on September 26th, Hurricane Helene made landfall at category 4 on the Saffir-Simpson scale on the panhandle of Florida, bringing high winds, extreme rainfall and storm surges to coastal areas. Over the next two days, it struck inland in a North-northeasterly direction, bringing further extreme rainfall to areas across most of Georgia, the western side of North and South Carolina, eastern Tennessee and southern Virginia. This led to extensive and in many cases unprecedented flash flooding across many of these regions. Over 230 people were killed and nearly 2 million were left without power (AP News, 2024; CNN, 2024).

Helene has caused widespread damage and disruption to critical infrastructure, including washed out roads, damaged water supply, power outages and communication disruption. Less than one-fifth of cellular sites were still down as of 6 October (FEMA, 2024), with over three million customers cut off from electricity in the Carolinas and Florida (Almasy, 2024; Yan & Almasy, 2024) and hundreds of roads including highways still impassable (NYT, 2024), hampering emergency services and aid.

Helene first began to take shape in the western Caribbean Sea around September 22nd, originating as a broad area of low pressure. Over the following days, as it gathered strength, the system was steered northward by prevailing atmospheric patterns, ultimately moving into the warm waters of the Gulf of Mexico. Once in the Gulf, Helene intensified into a hurricane. Despite traversing the Gulf over a relatively prolonged period, it maintained a consistent intensity, largely due to its sheer size and the dry air being drawn in from the west, which limited significant strengthening or weakening during this phase.

However, on September 26th, Helene experienced a period of rapid intensification just before making landfall. This sudden surge in strength was driven by a combination of highly favourable environmental conditions: The sea surface temperatures in the Gulf were exceptionally high, providing a source of heat and moisture to fuel the storm. Additionally, the mid-level wind shear, which can often disrupt a storm's structure, was unusually low, allowing Helene to maintain its organisation and deepen quickly. The atmosphere was also saturated with moisture, characterised by high relative humidity, which further contributed to the storm's explosive growth.

Not only the intensity of Helene was extreme but also the spatial extent. Helene's size with almost 400 miles across, similar in size to Katrina (The Conversation, 2024) placed it at the upper bounds of any hurricane seen in recent decades. Its vast wind field, coupled with its size, made it an exceptional storm in terms of scale and impact, distinguishing it from most tropical cyclones that had formed in the region over recent years.(NASA Earth Observation, 2024; NHC, 2024).

In the days leading up to Helene's landfall, a line of slow-moving storms formed along a stalled cold front, drawing in tropical moisture from Helene's outer edges. This system, stretching from Atlanta through the southern Appalachian region, led to very heavy rainfall in the southern states and Appalachia even before the heavy rainfall associated with Helene arrived. By midnight on the 26th, streamflows in the upstream, upslope areas of the Appalachians already recorded records.

The rain persisted throughout the 26th, as the frontal boundary remained nearly stationary, while Helene's outer rain bands began to approach, contributing additional moisture. Just when the main rainfall associated with Helene began to arrive mountain streams had overrun, water rushed down the rivers and into towns such as Asheville and caused landslides (NC State University, 2024).

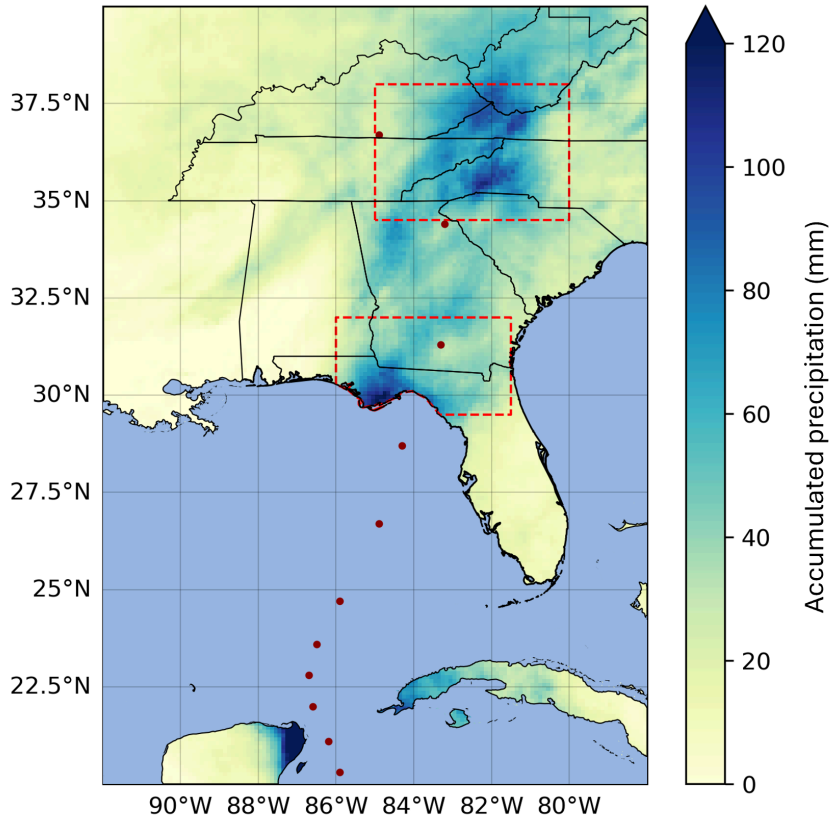

Figure 1.1: *Accumulated precipitation over the southeastern US from 25-27th September 2024. The track of Hurricane Helene is shown as a series of red points, and the red regions are those used for extreme rainfall analysis in section 2 of this report. The borders of the affected states are shown for reference. Data from IMERG.*

1.1 Hurricanes in southeastern USA

The North Atlantic (NA) hurricane season lasts from June-November and on average approximately 1-2 hurricanes make landfall in the US each year (NOAA, 2024). Hurricanes are some of the costliest disasters and between 1900-2017 there were 41 events that caused at least US$3 bn in damage (when adjusted to 2017 dollars), with the two most destructive events exceeding US$ 100 bn each (NHC, 2017). At the time of writing, up to date information on the most destructive hurricanes is not

accessible due to the impacts of Hurricane Helene on one of the National Centers of Environmental Information (NCEI) based in Asheville, North Carolina (NCEI, 2024). However, it is likely that Hurricane Ian in 2022 also crossed the US$100 bn threshold (NHC, 2022). While the increasing trend in damage due to such events is most strongly linked to increases in exposed assets to date, clearly any influence of climate change upon such events is of crucial societal relevance.

The influence of climate change on TCs varies by basin, as does the level of scientific evidence on these changes (Masson-Delmotte et al., 2021). On a global scale, recent decades have seen an increase in more intense TCs (category 3-5 on the Saffir-Simpson scale), but no change in the overall number of TCs. Recent studies on specific TCs as well as physical understanding suggest that extreme rainfall from TCs is increasing (Masson-Delmotte et al., 2021). This is explained partly by the Clausius-Clapeyron relation, which states that warmer air holds more moisture at a rate of 6-7% / °C. In the future, the proportion of the most intense TCs (categories 4-5) is projected to increase with further warming, as well as the average and maximum precipitation rates from these storms (Seneviratne et al., 2021).

Basin-specific changes are less certain, more variable and extend to other properties of TCs. For instance, in the NA, TCs making landfall over the contiguous US have slower translation speeds (Kossin, 2019) and are more frequently stalling or meandering, leading to more intense impacts as extreme conditions are sustained for longer periods over a given location (Seneviratne et al., 2021). In addition, NA hurricanes are increasing in both intensification rate and maximum intensity, which is unlikely to be explained by natural variability (Bhatia et al., 2019; Murakami et al., 2020).

Attribution studies now provide additional insight into the changing nature of hurricanes in a warming world. Hurricanes in the NA basin are the most frequently studied tropical cyclone events to date, with studies covering 8 recent events with combined damages of more than US$600 bn (at the time of occurrence) in the US and Caribbean. Almost across the board, rainfall from these events were amplified by anthropogenic climate change: Katrina in 2005 by 4%, Irma in 2017 by 6%, Maria in 2017 by 9% (Patricola and Wehner, 2018), Florence in 2018 by 5% (Reed et al., 2020), Dorian in 2019 by 5-18% (Reed et al., 2021), Ian in 2022 by 18% (Reed et al., 2023), and Harvey in 2017 by 7-38%. Changes in intensity are less clear than for rainfall, though one study using a pseudo global-warming approach found no detectable change in intensity to date but projected significantly increasing intensity at higher warming levels (Patricola and Wehner, 2018). Finally, during Hurricane Sandy in 2012, the effect of sea level rise due to climate change created a higher storm surge, directly leading to an additional US$8.1 bn in damages (Strauss et al., 2021).

1.2 Event Definition(s)

In this study, we characterise the event in several ways in order to capture both the environmental conditions leading to its intensity and the range of ways in which it led to impacts, including both extreme rainfall and high winds. This follows the same methodology as a recent rapid study on Typhoon Gaemi (World Weather Attribution, 2024). The report is broken into three sections.

First, the WWA protocol is applied to extreme rainfall across the affected region where impacts were reported. This is divided into two sections to reflect the changing character of the rainfall ; a coastal region in which rainfall was dominated by the tropical cyclone, and an inland region in which the remnants of the cyclone compounded the preceding rainfall event from a stalled cold front. This

analysis gives a probabilistic analysis of both precipitation extremes using a synthesis of observational and climate model products. The rainfall event definitions are as follows:

Rainfall:

- **Inland region:** June-November maximum 3-day accumulations over land areas within the region 34.5-38 °N and 80-85 °W (figure 1.1)
- **Coastal region:** June-November maximum 2-day accumulations over land areas within the region 29.5-32 °N and 81.5-86 °W (figure 1.1)

Second, we characterise the conditions that led to such an event using two different approaches. The potential intensity is a metric that predicts maximum typhoon wind speed using sea surface temperatures, sea level pressure, and temperature and humidity vertical profiles (Pérez-Alarcón et al., 2023; Emanuel, 1986). The potential intensity during the month of September is analysed in section 3 using the WWA method. The sea surface temperatures are also studied in isolation in section 4, using the Ocean Climate Shift Index. While it would be arguably more informative to study ocean heat content, doing so on a rapid basis was not feasible for this study given data availability, but future studies should strive to do so where possible. While potential intensity and SSTs are related, studying SSTs in isolation helps to disentangle the influence of climate change on the more complex overall potential intensity quantity. Further, using a combination of different approaches increases our confidence in the final resultant statement.

Environmental conditions:

1. **Potential intensity (PI):** June-September maximum of monthly mean PI averaged over ocean areas bounded by 82 - 89 °W, 15 - 35 °N (figure 1.2)
2. **Sea Surface Temperatures (SSTs):** 6-hourly SSTs at each point along the track of Hurricane Helene

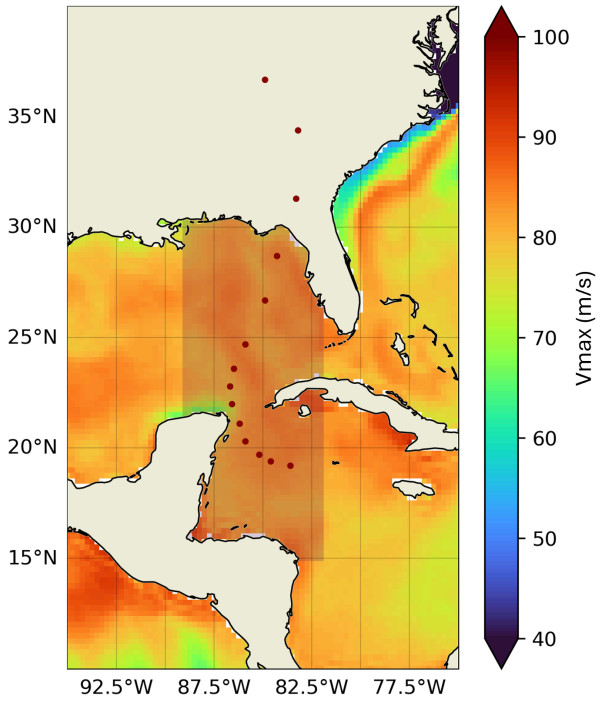

Figure 1.2: *September (1st-27th) mean potential intensity in the Caribbean sea and Gulf of Mexico. The study region is shaded and the track of Helene is shown as red points. Data from ERA5.*

Finally, in section 5, the attributable changes in wind speed intensity are assessed using a stochastic model of storm tracks and intensities.

Wind speeds:

1. **Florida landfall:** category 4 hurricanes making landfall in a region 2 degrees from Helene (figure 1.4)

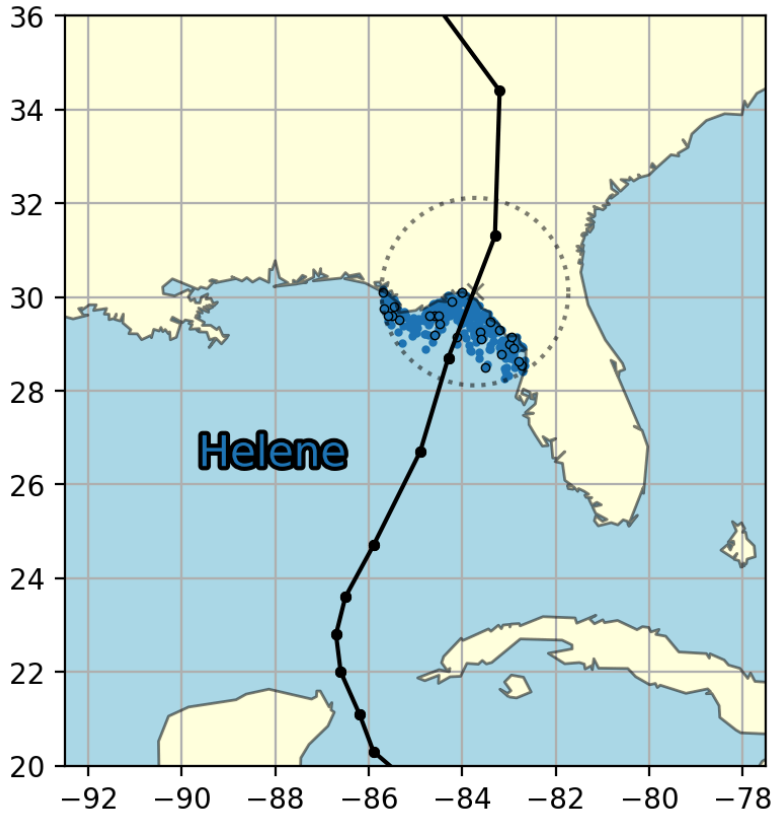

Figure 1.4: *Samples drawn from the IRIS dataset (blue dots) and historical landfall events in a region around the landfall of Hurricane Helene (track shown in black).*

For each event definition, we study the influence of anthropogenic climate change by comparing the likelihood and intensity of similar events at present with those in a 1.3 °C cooler climate. For the rainfall and potential intensity, we also extend this analysis into the future by assessing the influence of a further 0.7 °C of global warming from the present.

2 Extreme rainfall attribution using WWA protocol

The extreme rainfall events analysed in this section are as follows:

- **Inland region:** June-November maximum 3-day accumulations over land areas within the region 34.5-38 °N and 80-85 °W (figure 1.1)
- **Coastal region:** June-November maximum 2-day accumulations over land areas within the region 29.5-32 °N and 81.5-86 °W (figure 1.1)

2.1 Data and methods

2.1.1 Observational data

In this study, we use several observational and reanalysis datasets to characterise the extreme rainfall that occurred along the path of Hurricane Helene:

1. The European Centre for Medium-Range Weather Forecasts's 5th generation reanalysis product, ERA5, is a gridded dataset that combines historical observations into global estimates using advanced modelling and data assimilation systems (Hersbach et al., 2020). We use daily precipitation data from this product at a resolution of 0.25°, from the years 1950 to present. When the analysis was undertaken, reanalysis data was not yet available and given the complexity of the meteorology, the analysis data was not deemed reliable. As a result, the event itself was not included in this dataset, though it is still used to analyse trends over time.
2. We use CPC daily precipitation for the contiguous US region. This is the gridded product from NOAA PSL, Boulder, Colorado, USA known as the CPC Global Unified Daily Gridded data, available at 0.25° x 0.25° resolution, for the period 1979-present. Data are available from NOAA.
3. The Multi-Source Weighted-Ensemble Precipitation (MSWEP) v2.8 dataset (updated from Beck et al., 2019) is fully global, available at 3-hourly intervals and at 0.1° spatial resolution, available from 1979 to ~3 hours from real-time. This product combines gauge-, satellite-, and reanalysis-based data.
4. CHIRPS: The rainfall product developed by the UC Santa Barbara Climate Hazards Group called “Climate Hazards Group InfraRed Precipitation with Station data” (CHIRPS; Funk et al. 2015). Daily data are available at 0.05° resolution, from 1981-31 August 2024. The product incorporates satellite imagery with in-situ station data.

Finally, as a measure of anthropogenic climate change we use the (low-pass filtered) global mean surface temperature (GMST), where GMST is taken from the National Aeronautics and Space Administration (NASA) Goddard Institute for Space Science (GISS) surface temperature analysis (GISTEMP, Hansen et al., 2010 and Lenssen et al. 2019).

2.1.2 Model and experiment descriptions

We use 2 multi-model ensembles from climate modelling experiments using very different framings (Philip et al., 2020): Sea Surface temperature (SST) driven global circulation high resolution models, coupled global circulation models and regional climate models.

1. Coordinated Regional Climate Downscaling Experiment (CORDEX) - North America (CORDEX-NAM) data archive contains output from regional climate models (RCMs) run over a domain covering most of North America using boundary conditions from global climate model (GCM) simulations in the CMIP5 archive. These simulations run from 1950–2100 with a spatial resolution of 0.22°/25km or 0.44°/50km (Mearns et al., 2017), composed of historical simulations up to 2005, and extended to the year 2100 using the RCP8.5 scenario.

2. The FLOR (Vecchi et al., 2014) and AM2.5C360 (Yang et al., 2021, Chan et al., 2021) climate models are developed at Geophysical Fluid Dynamics Laboratory (GFDL). The FLOR model is an atmosphere-ocean coupled GCM with a resolution of 50 km for land and atmosphere and 1 degree for ocean and ice. Ten ensemble simulations from FLOR are analysed, which cover the period from 1860 to 2100 and include both the historical and RCP4.5 experiments driven by transient radiative forcings from CMIP5 (Taylor et al., 2012). AM2.5C360 is atmospheric GCM based on that in the FLOR model (Delworth et al., 2012, Vecchi et al., 2014) with a horizontal resolution of 25 km (and is referred to as 'AM2' throughout this text). Three ensemble simulations of the Atmospheric Model Intercomparison Project (AMIP) experiment (1871-2100) from each of the two models are analysed. Radiative forcings are using historical values over 1871-2014 and RCP4.5 values after that. Simulations are initialised from three different pre-industrial conditions but forced by the same SSTs from HadISST1 (Rayner et al., 2003) after groupwise adjustments (Chan et al., 2021) over 1871-2020. SSTs between 2021 and 2100 are using the FLOR RCP4.5 experiment 10-ensemble mean values after bias correction.

2.1.3 Statistical methods

Methods for observational and model analysis and for model evaluation and synthesis are used according to the World Weather Attribution Protocol, described in Philip et al., (2020), with supporting details found in van Oldenborgh et al., (2021), Ciavarella et al., (2021) and here. The key steps, presented in sections 3-6, are: (3) trend estimation from observations; (4) model validation; (5) multi-method multi-model attribution; and (6) synthesis of the attribution statement.

In this report we analyse time series of 2- and 3-day June-November maxima extreme rainfall over the study regions for a range of observational, reanalysis and model datasets. A nonstationary generalised extreme value (GEV) distribution is used to statistically model these variables. For precipitation, the distribution is assumed to scale exponentially with the covariate, with the dispersion (the ratio between the standard deviation and the mean) remaining constant over time.

For each time series we calculate the return periods, probability ratio (PR; the factor-change in the event's probability) and change in intensity of the event under study for the 2024 GMST and for 1.3 °C cooler GMST: this allows us to compare the climate of now and of the preindustrial past (1850-1900, based on the Global Warming Index). We also repeat the calculations for a 0.7 °C warmer GMST, allowing us to climate of now with a hypothetical future world of continued warming.

2.2 Observational analysis: return period and trend

2.2.1 Analysis of gridded data

The statistical model described in the previous section is fit to the time series of each extreme index from each observational dataset. This enables estimation of the return periods in the present day for an event of the magnitude observed during the passage of Hurricane Helene (table 2.1). There is very strong variation between regions in how extreme the rainfall was.

In the coastal region, regionally-averaged 2-day precipitation totals of ~95 mm have return periods of between 5.8-7.3 years. As a result, the 7 year event, at the upper end of the range of observational estimates, is studied in this analysis. In the inland region, the regionally-averaged 3-day summed precipitation was between 120-140 mm in the two datasets with record of the event at the time of study. This was a much rarer event, which is also evident from the rolling totals in figure 2.2 relative to figure 2.1, with both estimating return periods of approximately 70 years. The 70 year event was therefore selected for study.

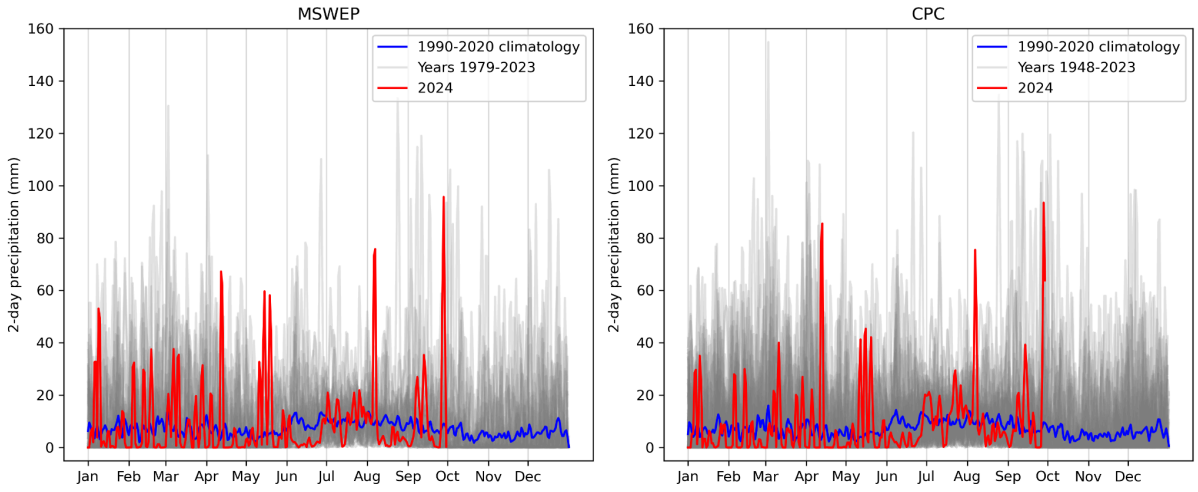

Figure 2.1: *2-day rolling precipitation totals in the coastal region around southern Georgia and northern Florida in two observational and reanalysis datasets, MSWEP (left) and CPC (right). Each year in the record is shown in grey, the 1990-2020 climatology in blue and 2024 in red. Hurricane Helene is clear as the final peak in each dataset.*

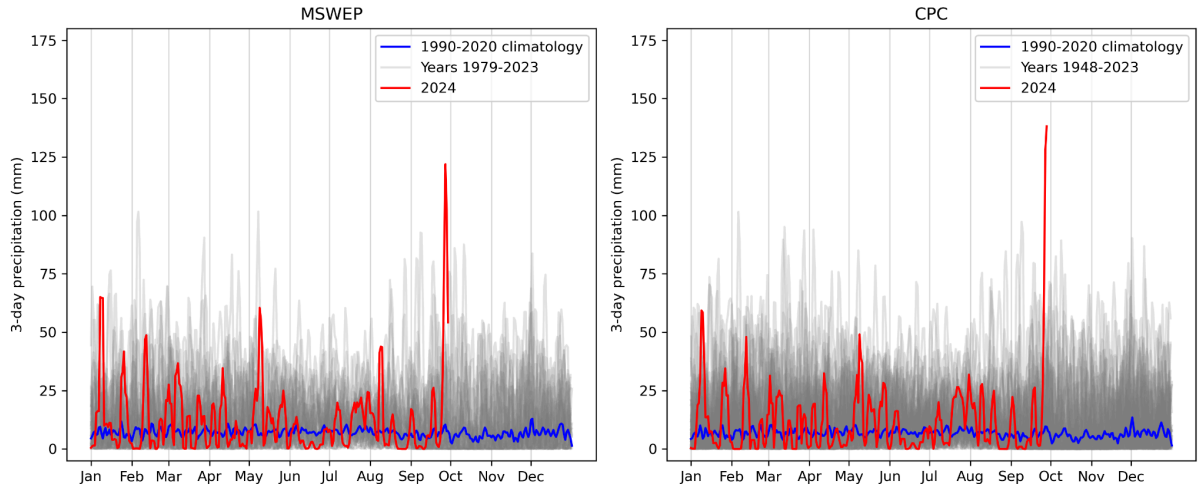

Figure 2.2: *3-day rolling precipitation totals in the inland region around western North Carolina and eastern Tennessee in two observational and reanalysis datasets, MSWEP (left) and CPC (right). Each year in the record is shown in grey, the 1990-2020 climatology in blue and 2024 in red. Hurricane Helene is clear as the final peak in each dataset.*

Dataset	Coastal region extreme 2-day rainfall		Inland region extreme 3-day rainfall	
	Magnitude (mm)	Return period (95% C.I.)	Magnitude (mm)	Return period (95% C.I.)
CPC	138.1	5.8 (2.9 - 15.1)	93.5	67.6 (22.8-inf)
MSWEP	121.9	7.3 (2.7 - 23.4)	95.7	71.9 (21.0-2800)
Return periods		**7**		**70**

Table 2.1: *Estimated return periods of extreme rainfall events as characterised in two regions, coastal and inland, over the southeastern US in the CPC and MSWEP reanalysis datasets with coverage of the event.*

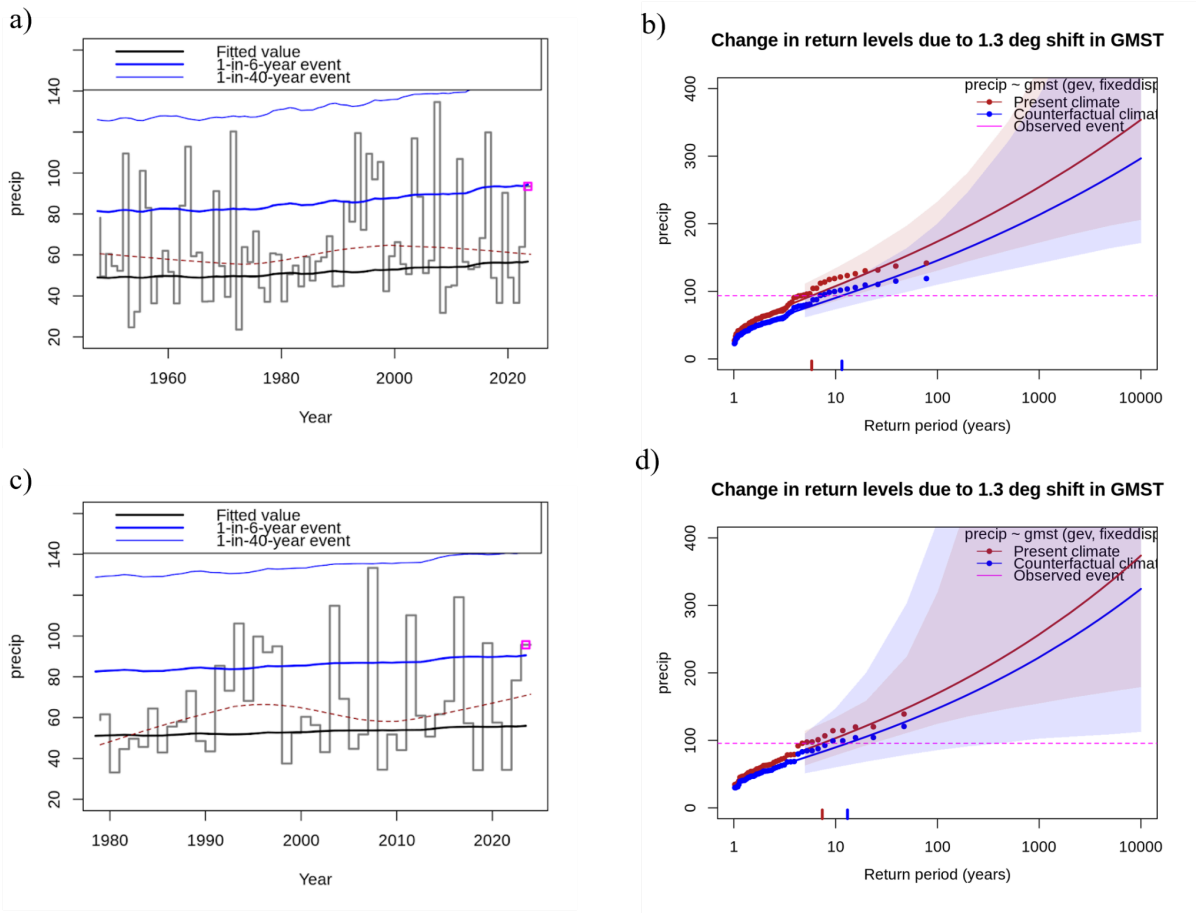

Figure 2.3: *Time series (left) and statistical fits (right) to June-November maxima of 2-day accumulated precipitation in the coastal region affected by Hurricane Helene, in CPC (top) and MSWEP (lower). The influence of GMST is shown with the black line on the trend plots and the red vs blue probability curves. The magnitude of the is highlighted with a purple box (left) and line (right).*

Dataset	Coastal region 2-day extreme rainfall		GMST trend	
	Magnitude (mm)	Return period (95% C.I.)	Probability Ratio	Change in magnitude (%)
CPC	93.5	5.8 (2.9 - 15.1)	2.0 (0.5-10)	19.3 (-14.6 - 71.8)
MSWEP	95.7	7.3 (2.7 - 23.4)	1.8 (0.2 - 130.7)	15.2 (-40.6 - 109.1)
CHIRPS*	84.7	7	5.8 (0.1 - inf)	20.8 (-29.2 - 103.2)
ERA5*	89.7	7	2.8 (1.0 - 11.2)	31.2 (1.1 - 78.1)

Table 2.2: *Change in probability ratio and magnitude for extreme rainfall in the coastal region in which Helene made landfall, due to GMST. Light blue indicates a wetting trend that crosses no change, dark blue indicates a statistically significant wetting trend, and grey indicates that the value is not used for subsequent analysis. *ERA5 and CHIRPS did not have the event included in the fit and instead were evaluated for a 7-year return period event.*

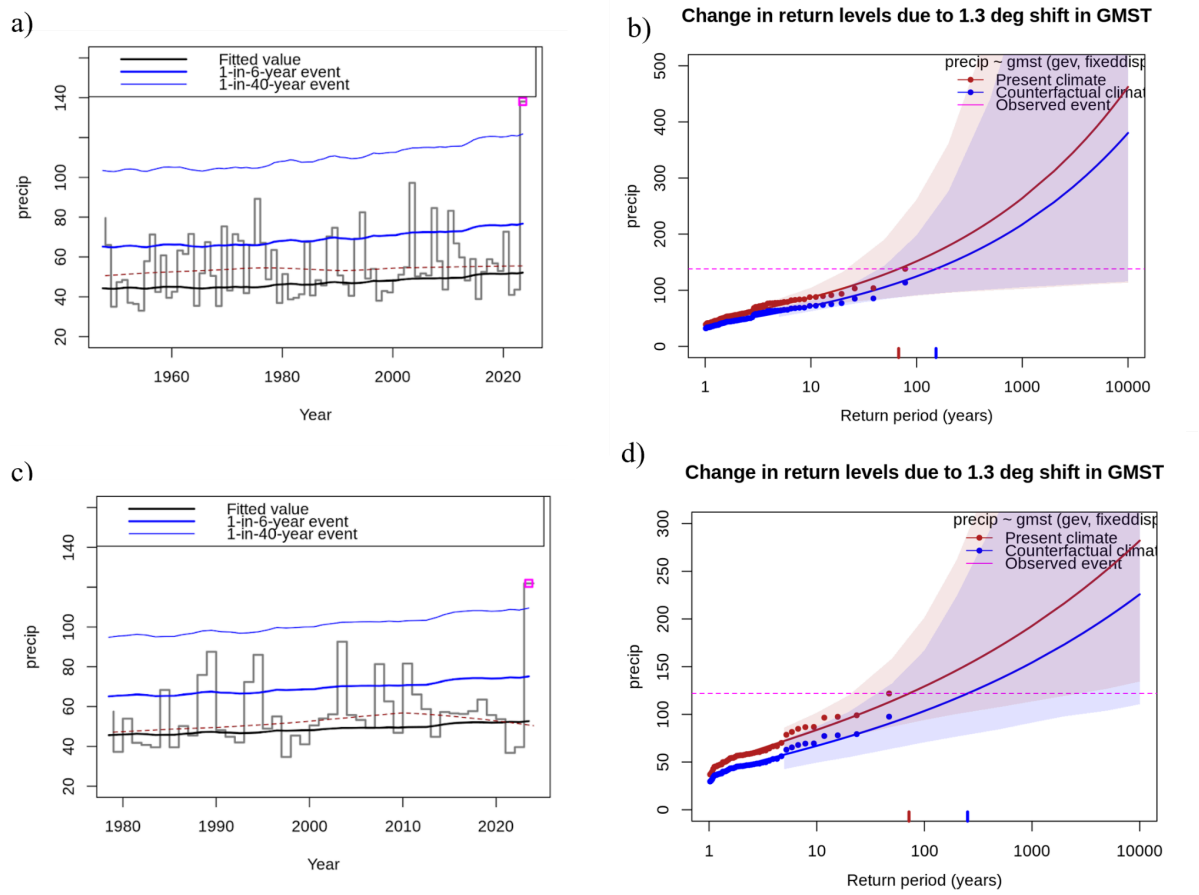

Figure 2.4: *Time series (left) and statistical fits (right) to June-November maxima of 3-day accumulated precipitation in the inland region affected by Hurricane Helene, in CPC (top) and MSWEP (lower). The influence of GMST is shown with the black line on the trend plots and the red vs blue probability curves. The magnitude of the is highlighted with a purple box (left) and line (right).*

Dataset	Inland region 3-day extreme rainfall		GMST trend	
	Magnitude (mm)	Return period (95% C.I.)	Probability Ratio	Change in magnitude (%)
CPC	138.1	67.6 (22.8-inf)	2.3 (0.4-10.1)	21.6 (-5.6 - 54.5)
MSWEP	121.9	71.9 (21.0-2800)	3.5 (0.5 - 143.4)	24.9 (-11.7 - 89.1)
CHIRPS*	95.2	70	80.2 (0-inf)	12.3 (-25.4 - 70.3)
ERA5*	111.0	70	3.8 (0.7 - 147.3)	20.1 (-4.9 - 56.3)

Table 2.3: *Change in probability ratio and magnitude for extreme rainfall in an inland region in which Helene drove extensive flooding due to GMST. Light blue indicates a wetting trend that crosses no change, grey indicates that the value is not used for subsequent analysis. *ERA5 and CHIRPS did not have the event included in the fit and instead were evaluated for a 70-year return period event.*

Overall in observations, compared to a preindustrial climate,present levels of warming resulted in an increase in likelihood and intensity of rainfall in both regions (tables 2.2 & 2.3). Across all datasets, only ERA5 gives statistically significant increases, and only in the coastal region. Further, CHIRPS gives extremely broad estimates of the changes in probability ratio with uncertainty bounds ranging from 0 (or close to 0) and infinite. It is therefore excluded from the synthesis of changes in likelihood. Despite these factors, the consistency of the signal across all datasets increases our confidence in a qualitative increase in similar extremes due to warming. Synthesising these results, we find that the overall observed increase due to warming by a factor of 2 in PR and 22% in intensity for the coastal region, and a factor of 3 in PR and 20% in intensity for the inland region (table 6.1). However, uncertainties for individual datasets are very large, suggesting that model analysis is also needed to refine this estimate.

2.3 Model evaluation

In this section we show the results of the model evaluation for the assessed region. The climate models are evaluated against the observations in their ability to capture:

1. Seasonal cycles: For this, we qualitatively compare the seasonal cycles based on model outputs against observations-based cycles. We discard the models that exhibit ill-defined peaks in their seasonal cycles. We also discard the model if the rainy season onset/termination varies significantly from the observations.

2. Spatial patterns: Models that do not match the observations in terms of the large-scale precipitation patterns are excluded.

3. Shape and dispersion parameters of the fitted statistical models. We discard the model if the model and observation parameters ranges do not overlap.

The models are labelled as ‘good’,’reasonable’, or ’bad’ based on their performances in terms of the three criteria discussed above. A model is given an overall rating of ‘good’ if it is rated ‘good’ for all three characteristics. If there is at least one ‘reasonable’, then its overall rating will be ‘reasonable’ and ‘bad’ if there is at least one ‘bad’.

Per framing or model setup we also use models that only just pass the validation tests if we only have five models or less for that framing that perform well. The tables show the model validation results.

2.3.1 Coastal region

Model / Observations	**Seasonal cycle**	**Spatial pattern**	**Dispersion**	**Shape parameter**	**Conclusion**
CPC			0.358 (0.284 ... 0.408)	0.093 (-0.054 ... 0.28)	
MSWEP			0.325 (0.239 ... 0.389)	0.13 (-0.16 ... 0.57)	
ERA5			0.340 (0.267 ... 0.387)	0.17 (-0.0051 ... 0.40)	
CORDEX					
CanESM2_rcp85_r1i1p1_CanRCM4_r2 (1)	good	good	0.344 (0.239 ... 0.410)	0.040 (-0.26 ... 0.41)	good
CanESM2_rcp85_r1i1p1_CRCM5_v1 (1)	good	reasonable	0.225 (0.153 ... 0.273)	0.18 (-0.086 ... 0.54)	reasonable
CNRM-CM5_rcp85_r1i1p1_CRCM5_v1 (1)	good	good	0.411 (0.328 ... 0.468)	-0.089 (-0.41 ... 0.18)	reasonable
GFDL-ESM2M_rcp85_r1i1p1_CRCM5_v1 (1)	good	reasonable	0.296 (0.219 ... 0.349)	-0.24 (-0.51 ... 0.087)	reasonable
GFDL-ESM2M_rcp85_r1i1p1_WRF_v3-5-1 (1)	good	reasonable	0.243 (0.187 ... 0.282)	-0.063 (-0.37 ... 0.22)	reasonable

HadGEM2-ES_rcp85_r1i1p1_WRF_v3-5-1 (1)	good	reasonable	0.228 (0.170 ... 0.270)	0.12 (-0.18 ... 0.50)	reasonable
MPI-ESM-LR_rcp85_r1i1p1_CRCM5_v1 (1)	good	reasonable	0.322 (0.235 ... 0.377)	-0.0053 (-0.33 ... 0.35)	reasonable
MPI-ESM-LR_rcp85_r1i1p1_RegCM4_v4-4-rc8 (1)	reasonable	good	0.244 (0.179 ... 0.284)	0.090 (-0.21 ... 0.39)	reasonable
MPI-ESM-LR_rcp85_r1i1p1_WRF_v3-5-1 (1)	good	reasonable	0.181 (0.104 ... 0.223)	0.16 (-0.044 ... 0.56)	bad
MPI-ESM-MR_rcp85_r1i1p1_CRCM5_v1 (1)	good	reasonable	0.258 (0.195 ... 0.302)	0.0061 (-0.30 ... 0.26)	reasonable
FLOR ensemble (10)					good
pr2day_1 ()	good	good	0.291 (0.213 ... 0.340)	0.0057 (-0.18 ... 0.32)	good
pr2day_10 ()	good	good	0.269 (0.164 ... 0.319)	0.19 (-0.14 ... 0.86)	good
pr2day_2 ()	good	good	0.305 (0.186 ... 0.367)	0.12 (-0.17 ... 0.71)	good
pr2day_3 ()	good	good	0.247 (0.189 ... 0.288)	-0.21 (-0.44 ... 0.021)	reasonable
pr2day_4 ()	good	good	0.327 (0.260 ... 0.373)	0.0026 (-0.27 ... 0.32)	good
pr2day_5 ()	good	good	0.314 (0.240 ... 0.374)	-0.013 (-0.39 ... 0.21)	good
pr2day_6 ()	good	good	0.273 (0.191 ... 0.331)	-0.14 (-0.70 ... 0.29)	good
pr2day_7 ()	good	good	0.257 (0.182 ... 0.300)	-0.039 (-0.33 ... 0.21)	good
pr2day_8 ()	good	good	0.281 (0.217 ... 0.323)	-0.0021 (-0.30 ... 0.29)	good
pr2day_9 ()	good	good	0.284 (0.211 ... 0.336)	-0.015 (-0.27 ... 0.20)	good
AM2.5C360 ensemble (3)					reasonable
pr2day_6 ()	good	reasonable	0.343 (0.247 ... 0.410)	0.27 (-0.021 ... 0.63)	reasonable
pr2day_7 ()	good	reasonable	0.318 (0.231 ... 0.378)	0.14 (-0.27 ... 0.46)	reasonable
pr2day_8 ()	good	reasonable	0.237 (0.168 ... 0.292)	0.41 (0.13 ... 0.74)	reasonable

Table 2.4: *Evaluation of the climate models considered for attribution of rainfall over the coastal US region. For each model, the best estimate of the dispersion and shape parameters are shown and a 95% confidence interval for each, obtained via bootstrapping. The qualitative evaluation is shown in the right-hand column.*

2.3.2 Inland region

Model / Observations	Seasonal cycle	Spatial pattern	Dispersion	Shape parameter	Conclusion
CPC			0.223 (0.175 ... 0.261)	0.25 (-0.14 ... 0.55)	
MSWEP			0.220 (0.144 ... 0.259)	0.15 (-0.047 ... 0.47)	
ERA5			0.251 (0.200 ... 0.288)	0.056 (-0.11 ... 0.20)	
CORDEX					
CanESM2_rcp85_r1i1p1_CanRCM4_r2 (1)	good	good	0.222 (0.165 ... 0.266)	-0.44 (-0.76 ... -0.021)	reasonable
CanESM2_rcp85_r1i1p1_CRCM5_v1 (1)	good	reasonable	0.202 (0.144 ... 0.237)	0.037 (-0.21 ... 0.40)	reasonable
CNRM-CM5_rcp85_r1i1p1_CRCM5_v1 (1)	good	good	0.192 (0.142 ... 0.232)	0.12 (-0.26 ... 0.45)	good
GFDL-ESM2M_rcp85_r1i1p1_CRCM5_v1 (1)	good	reasonable	0.167 (0.130 ... 0.198)	-0.18 (-0.49 ... 0.020)	reasonable
GFDL-ESM2M_rcp85_r1i1p1_WRF_v3-5-1 (1)	reasonable	reasonable	0.192 (0.147 ... 0.227)	-0.37 (-0.77 ... 0.015)	reasonable
HadGEM2-ES_rcp85_r1i1p1_WRF_v3-5-1 (1)	reasonable	reasonable	0.197 (0.137 ... 0.242)	0.20 (-0.016 ... 0.52)	reasonable
MPI-ESM-LR_rcp85_r1i1p1_CRCM5_v1 (1)	good	reasonable	0.227 (0.173 ... 0.261)	0.074 (-0.27 ... 0.40)	reasonable
MPI-ESM-LR_rcp85_r1i1p1_RegCM4_v4-4-rc8 (1)	good	good	0.248 (0.178 ... 0.295)	0.027 (-0.27 ... 0.21)	good
MPI-ESM-LR_rcp85_r1i1p1_WRF_v3-5-1 (1)	good	reasonable	0.187 (0.146 ... 0.222)	-0.46 (-0.83 ... -0.17)	bad
MPI-ESM-MR_rcp85_r1i1p1_CRCM5_v1 (1)	good	reasonable	0.262 (0.167 ... 0.325)	-0.058 (-0.33 ... 0.30)	reasonable
FLOR ensemble (10)					reasonable
pr3day_1 ()	reasonable	good	0.211 (0.126 ... 0.253)	0.16 (-0.30 ... 0.71)	reasonable
pr3day_10 ()	reasonable	good	0.188 (0.145 ... 0.220)	-0.019 (-0.33 ... 0.24)	reasonable
pr2day_2 ()	reasonable	good	0.185 (0.137 ... 0.217)	-0.042 (-0.28 ... 0.19)	reasonable
pr2day_3 ()	reasonable	good	0.253 (0.201 ... 0.297)	-0.010 (-0.30 ... 0.23)	reasonable
pr2day_4 ()	reasonable	good	0.233 (0.176 ... 0.275)	-0.082 (-0.42 ... 0.32)	reasonable

pr2day_5 ()	reasonable	good	0.204 (0.142 ... 0.248)	0.079 (-0.23 ... 0.48)	reasonable
pr2day_6 ()	reasonable	good	0.228 (0.175 ... 0.265)	0.090 (-0.30 ... 0.43)	reasonable
pr2day_7 ()	reasonable	good	0.189 (0.146 ... 0.226)	-0.064 (-0.43 ... 0.20)	reasonable
pr2day_8 ()	reasonable	good	0.191 (0.151 ... 0.225)	-0.053 (-0.35 ... 0.23)	reasonable
pr2day_9 ()	reasonable	good	0.176 (0.116 ... 0.218)	0.075 (-0.22 ... 0.47)	reasonable
AM2.5C360 ensemble (3)					reasonable
pr2day_6 ()	reasonable	reasonable	0.252 (0.192 ... 0.289)	0.15 (-0.16 ... 0.47)	reasonable
pr2day_7 ()	reasonable	reasonable	0.295 (0.222 ... 0.346)	-0.042 (-0.37 ... 0.16)	reasonable
pr2day_8 ()	reasonable	reasonable	0.282 (0.207 ... 0.325)	-0.036 (-0.48 ... 0.49)	reasonable

Table 2.5: *Evaluation of the climate models considered for attribution of rainfall over the inland US region. For each model, the best estimate of the dispersion and shape parameters are shown and a 95% confidence interval for each, obtained via bootstrapping. The qualitative evaluation is shown in the right-hand column.*

2.4 Multi-method multi-model attribution

This section shows Probability Ratios and change in intensity ΔI for models that passed model evaluation and also includes the values calculated from the fits with observations.

2.4.1 Coastal region

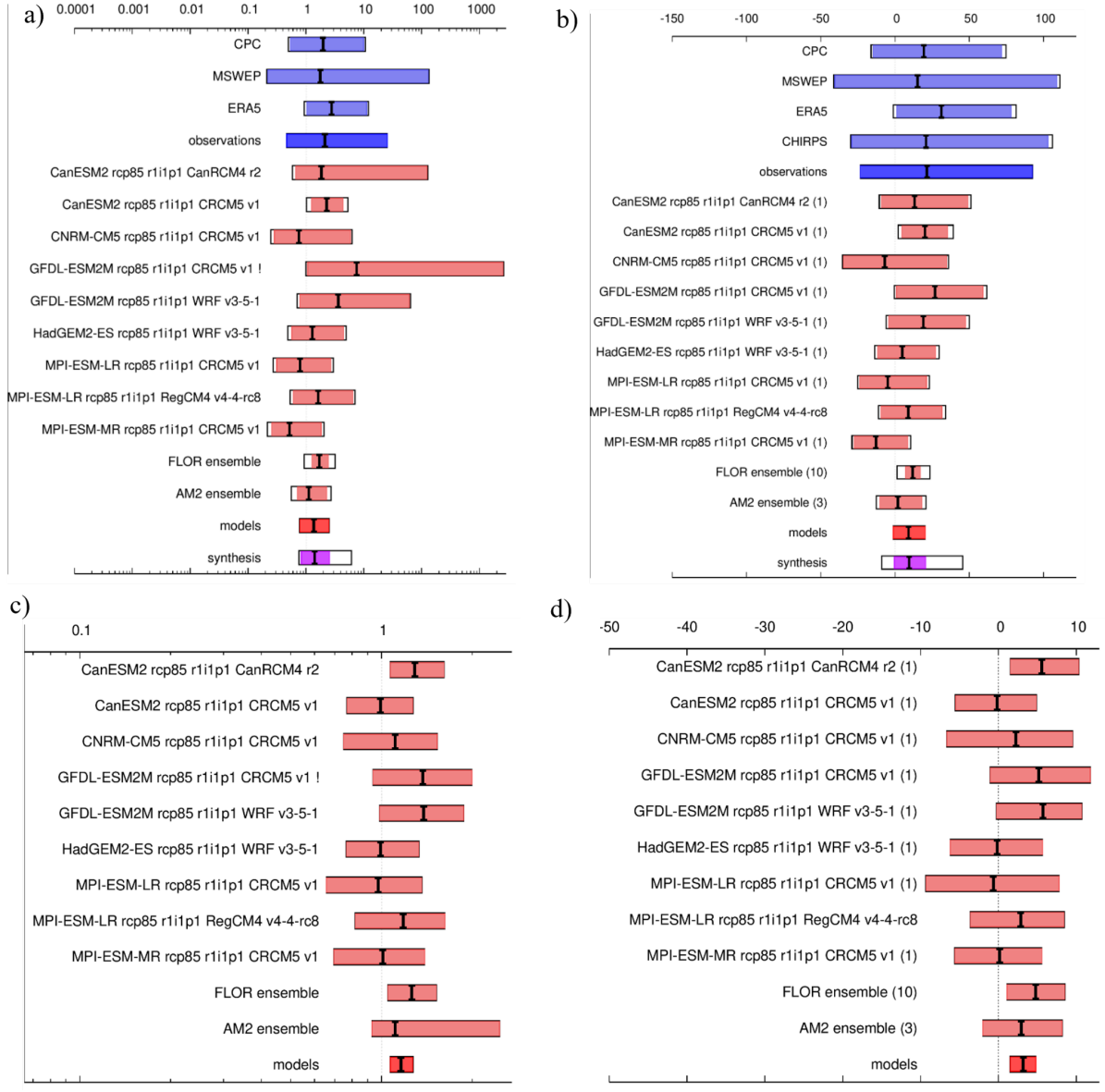

Figure 2.5: *Synthesised changes for a 7-year 2-day JJASON maximum rainfall event over the coastal region domain due to GMST. Changes in PR (left) and intensity (right) are shown for a historical period comparing the past 1.3°C cooler climate with the present (top row) and for a future period, based on model projections only, comparing the present and a 2°C warmed climate (bottom row). Note: AM2 refers to the AM2.5C360 ensemble described in section 2.1.2.*

.

2.4.2 Inland region

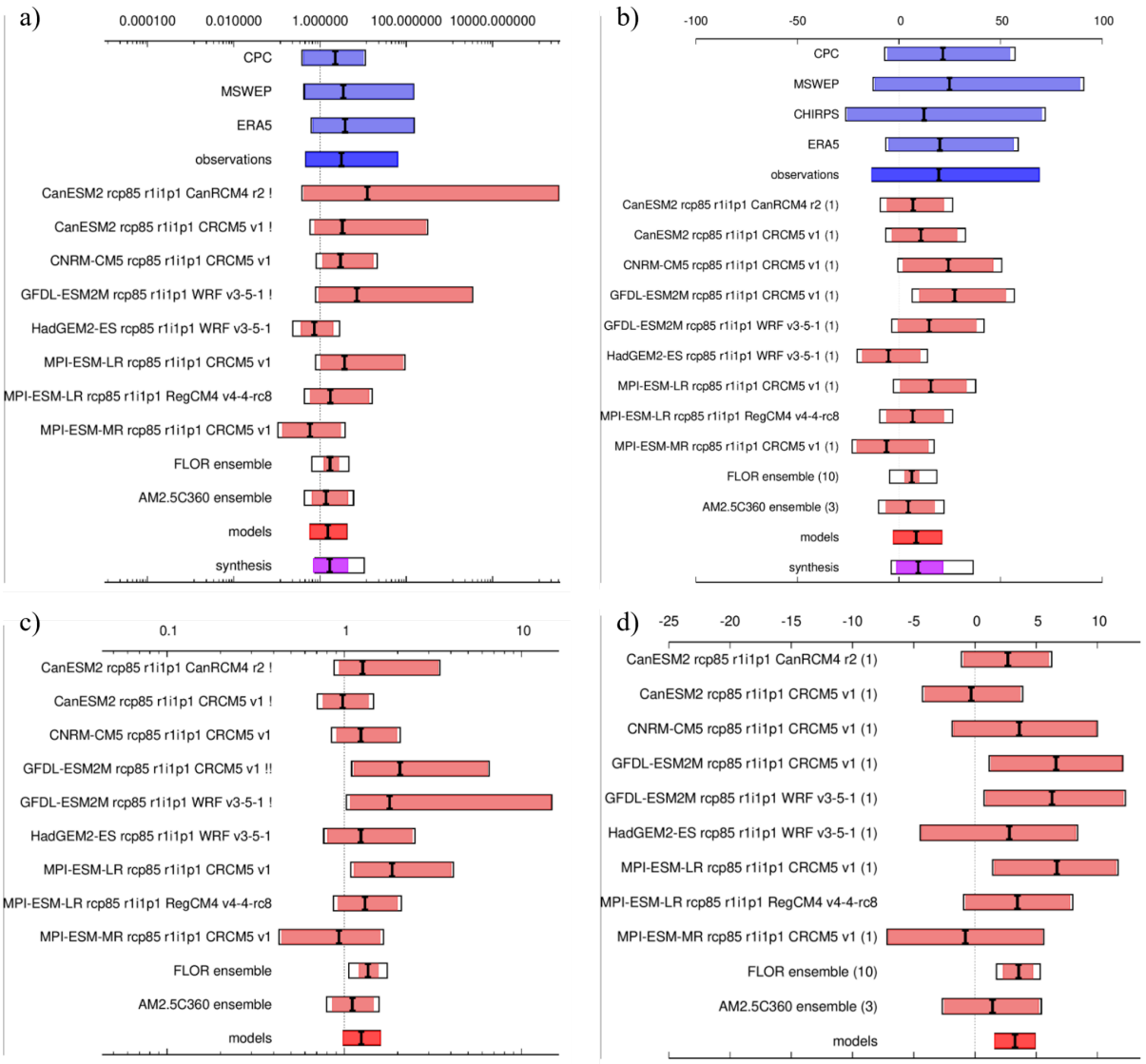

Figure 2.6: *Synthesised changes for a 70-year 3-day JJASON maximum rainfall event over the inland region domain due to GMST. Changes in PR (left) and intensity (right) are shown for a historical period comparing the past 1.3°C cooler climate with the present (top row) and for a future period, based on model projections only, comparing the present and a 2°C warmed climate (bottom row).*

3 Potential Intensity attribution using WWA protocol

The event definitions studied in this section are as follows:

1. **Potential intensity (PI):** June-November maximum of monthly mean PI over a ocean areas bounded by 82-89 °W, 15-35 °N (figure 1.3)

3.1 Data and methods

3.1.1 Observational data

ERA5 (Hersbach et al., 2020) is used to analyse the anthropogenic influence upon the conditions leading to Hurricane Helene. We use sea surface temperatures, sea level pressure, and specific humidity and atmospheric temperatures at all available pressure levels from this product. The Potential Intensity is calculated from these variables using the open-source PyPI package (Gilford, 2021).

As in the previous section, as a measure of anthropogenic climate change we use the (low-pass filtered) global mean surface temperature (GMST), where GMST is taken from the National Aeronautics and Space Administration (NASA) Goddard Institute for Space Science (GISS) surface temperature analysis (GISTEMP, Hansen et al., 2010 and Lenssen et al. 2019).

3.1.2 Model and experiment descriptions

To estimate the influence of anthropogenic climate change upon the potential intensity in which Helene occurred, we use the CMIP6 multi-model ensemble. This consists of simulations from 11 participating models with varying resolutions. For more details on CMIP6, please see Eyring et al., (2016). For all simulations, the period 1850 to 2015 is based on historical simulations, while the SSP5-8.5 scenario is used for the remainder of the 21st century.

3.1.3 Statistical methods

The methods for attribution of the extreme indices detailed above are the same as set out in section 2.1.3 with a few minor changes. A nonstationary Gaussian distribution is used to model each of these indices. For PI, the distribution is assumed to shift linearly with the covariate GMST, while the variance remains constant.

3.2 Observational analysis: return period and trend

3.2.1 Analysis of gridded data

The statistical model described in sections 2.1.3 and 3.1.3 is fit to the time series (figure 3.1) of each extreme index from the observational dataset ERA5. This enables estimation of the return periods in

the present day for an event of the observed magnitude at the time of Hurricane Helene (table 3.1). The potential intensity in the region of Hurricane Helene is very common in the current climate with a return period of 3 years.

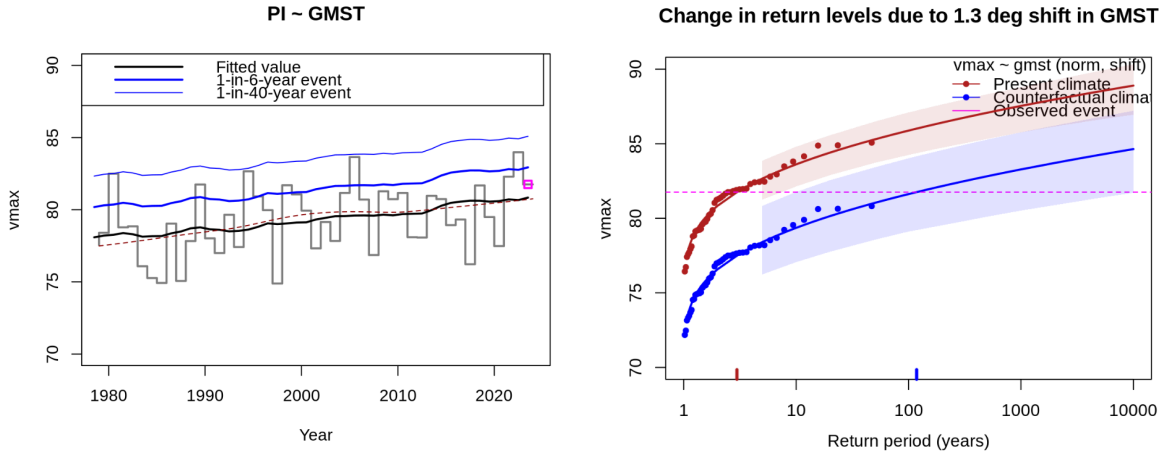

Figure 3.1: *Time series of September potential intensity, averaged over an area around the track of Hurricane Helene. Data from ERA5.*

Figure 3.1 shows the time series and changing return period of PI in the region as a monthly maximum each June-September since 1979. By varying the covariate GMST between its present and pre industrial levels, the probability ratio and change in magnitude of 2024-like events are estimated (table 3.1). As expected from figure 3.1, the PI index exhibits a strong and statistically significant increasing trend with warming. The PI in September 2024 has become around 40 times more likely, suggesting that it was previously a 1 in 120 year event. Equivalently, the maximum wind velocity became roughly 4 m/s stronger.

Dataset	Return period	Probability Ratio	Change in magnitude (m/s)
ERA5	2.97 (1.71 - 7.27)	39.6 (1.8 - 5437)	4.26 (0.81 - 7.28)

Table 3.1: *Return period, change in probability ratio and magnitude for the potential intensity in September 2024 in a region around the track of Hurricane Helene, due to GMST. Dark blue indicates a statistically significant increasing trend.*

3.3 Model evaluation

In the subsections below we show the results of the model evaluation for each location (individual figures shown in appendix A.1). The model evaluation steps are the same as set out in section 2.3. The tables show the model evaluation results.

3.3.1 Potential intensity

Of the 11 CMIP6 models analysed, 6 were rated ‘bad’ and discarded from the attribution analysis. No models performed well across all criteria, so all 5 remaining models were used.

Model / Observations	**Seasonal cycle**	**Spatial pattern**	**Sigma**	**Conclusion**
ERA5			2.17 (1.74 ... 2.44)	
CMIP6				
ACCESS-CM2 (1)	bad	good	3.24 (2.68 ... 3.64)	bad
BCC-CSM2-MR (1)	reasonable	reasonable	2.73 (1.89 ... 3.42)	reasonable
CanESM5 (1)	good	reasonable	2.94 (2.36 ... 3.35)	reasonable
CMCC-ESM2 (1)	reasonable	reasonable	1.78 (1.33 ... 2.05)	reasonable
INM-CM5-0 (1)	reasonable	good	1.28 (0.966 ... 1.51)	bad
KIOST-ESM (1)	reasonable	reasonable	3.27 (2.50 ... 3.87)	bad
MIROC6 (1)	good	bad	3.65 (2.88 ... 4.31)	bad
MPI-ESM1-2-LR (1)	bad	reasonable	2.27 (1.64 ... 2.75)	bad
NESM3 (1)	reasonable	bad	3.57 (2.59 ... 4.26)	bad
NorESM2-LM (1)	reasonable	reasonable	2.52 (1.96 ... 3.00)	reasonable
NorESM2-MM (1)	reasonable	reasonable	2.70 (2.17 ... 3.11)	reasonable

Table 3.3: *Evaluation of the climate models considered for attribution of potential intensity around the track of Helene. For each model, the best estimate of the sigma parameter is shown with a 95% confidence interval, obtained via bootstrapping. The qualitative evaluation is shown in the right-hand column.*

3.4 Multi-method multi-model attribution

This section shows Probability Ratios and change in intensity ΔI for models that passed model evaluation and also includes the values calculated from the fits with observations. The synthesis process (to produce figure 3.2) is conducted as set out in section 2.4. The synthesised results are also tabulated in section 6 alongside the other hazard sections for ease of comparison.

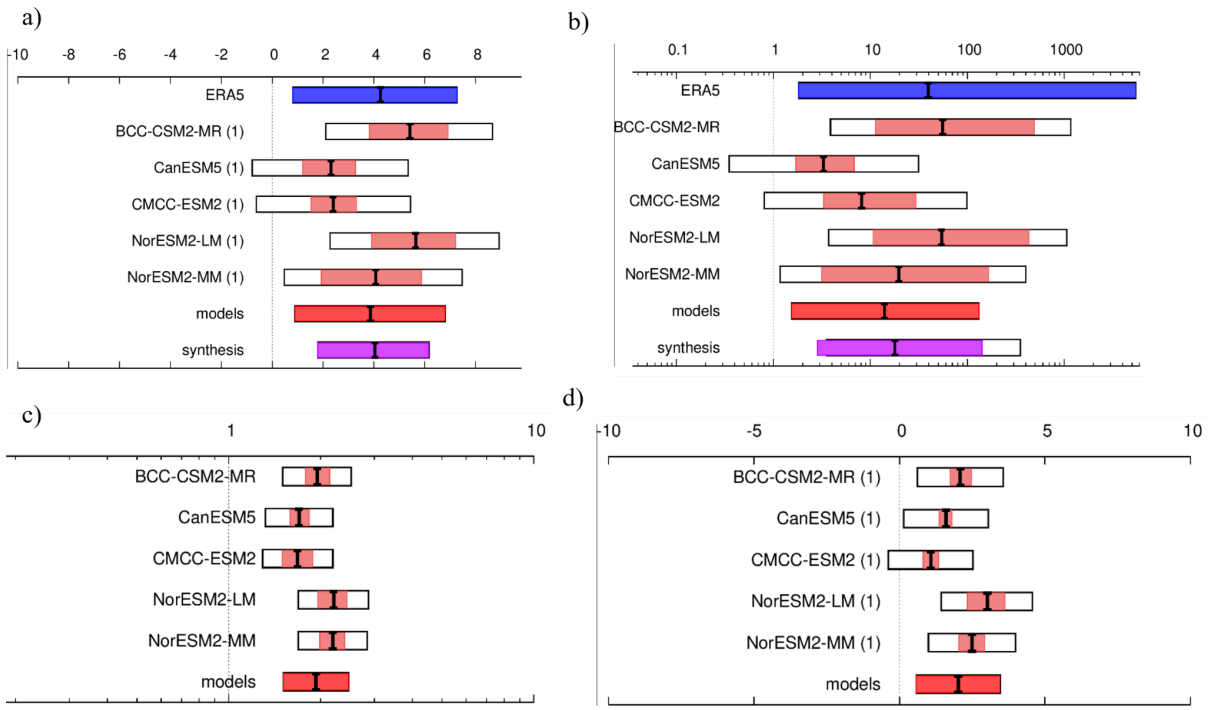

Figure 3.2: *Synthesised changes for a 3-year September mean potential intensity event in a region around Helene's track due to GMST. Changes in PR (left) and intensity (right) are shown for a historical period comparing the past 1.3°C cooler climate with the present (top row) and for a future period, based on model projections only, comparing the present and a 2°C warmed climate (bottom row)*

4 Sea Surface Temperatures along Helene's track

4.1 Data and Methods

Climate Central's Climate Shift Index: Ocean (Ocean CSI) tool is used to rapidly compute the influence of human-caused climate change on Sea Surface Temperatures along Hurricane Helene's track. The methodology underpinning this attribution tool is based on peer-reviewed research (Giguere et. al, 2024). It uses a combination of an empirically-driven attribution method using OISST data (Huang et. al, 2021), and model simulations using an ensemble of 13 debiased CMIP6 models. Results from these two methods are aggregated to compute a single metric measuring the increase in likelihood of an SST occurring as a result of climate change. This metric, called the Ocean CSI, is the ratio of the probability of a temperature occurring in today's climate to the probability of that same temperature occurring in a world without human-caused climate change. In addition to likelihood changes, the methods used to compute the Ocean CSI can be used to measure the temperature increase in a location on a given day due to climate change (Giguere et. al, 2024). This allows us to calculate the specific difference between an observed daily temperature in a location and what that temperature would have been in a counterfactual world without climate change. We estimate both the Ocean CSI and this climate-driven warming along Hurricane Helene's track and in the surrounding region. The Ocean CSI uses 0.25° by 0.25° latitude-longitude grid cells. For each point along the track, we found the cell and corresponding daily metrics closest to the centre of the storm at that time.

4.2 Attribution Analysis

On average, temperatures along the track were made 1.26°C (2.3°F) warmer by human caused climate change (Fig. 4.1). The strongest climate-driven warming occurred early on in the life cycle of Hurricane Helene, while it was still developing into a tropical storm.

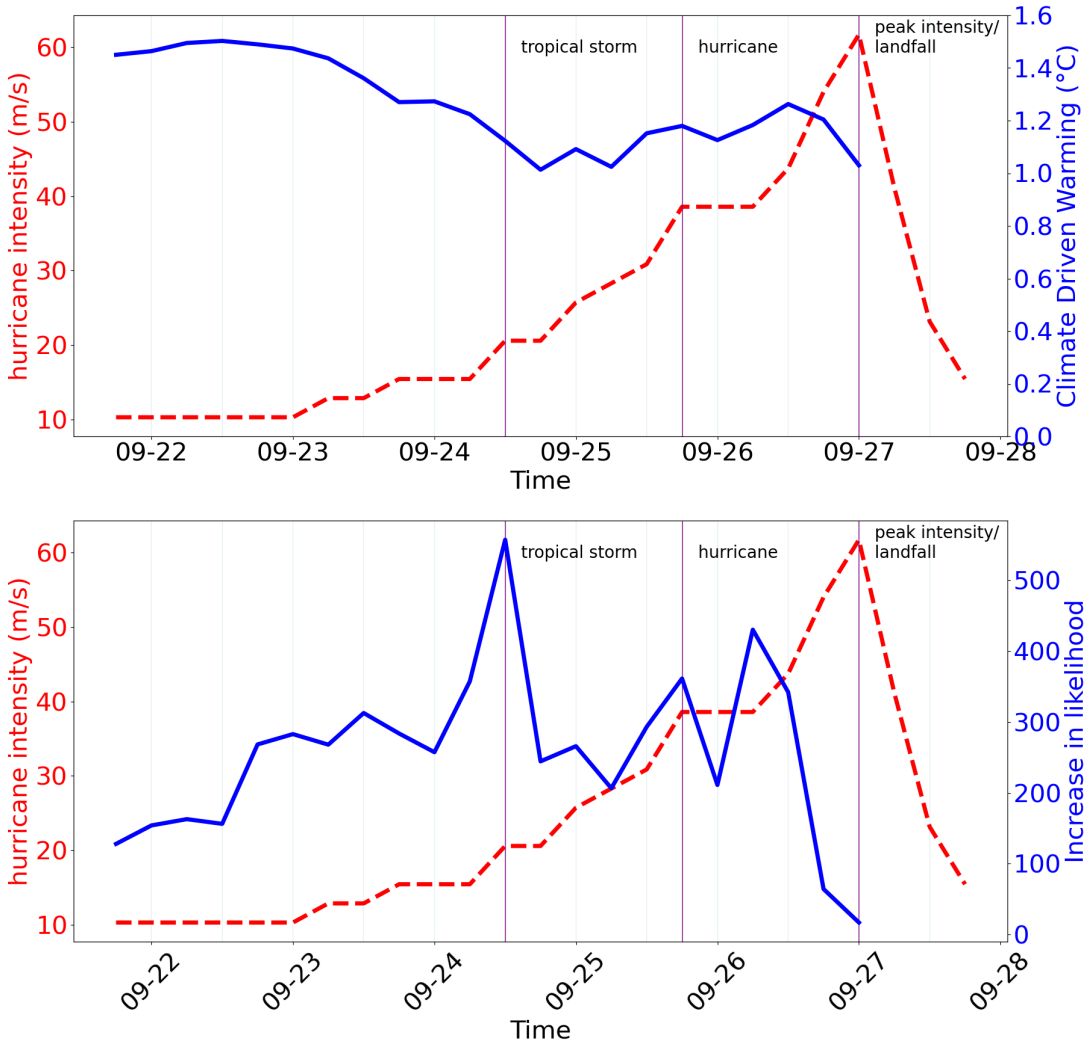

Figure 4.1: *Climate driven warming (top) and increase in likelihood of sea surface temperatures occurring as a result of climate change (bottom). Data from Climate Central Ocean CSI. Additionally, both figures present hurricane intensity (as a red, dashed line).*

However, Ocean CSI reached its highest value (557) when it developed into a tropical storm on September 24th (Figure 4.2). This indicates that the temperatures present while Helene was developing into a tropical storm were made more than 557 times more likely to occur today than in a world without climate change. On average, temperatures along hurricane Helene's lifetime from disturbance to landfall were made 255 times more likely to occur as a result of climate change. In the hours prior to making landfall, both the climate driven warming and the Ocean CSI decreased relative to their earlier peaks. But prior to landfall, temperatures were still 1.0°C higher than they would have been without human-caused climate change, and the observed temperatures were made 17 times more likely to occur as a result of climate change.

These results are consistent with our expectation, given the strong and reliable connection between observed SSTs and global mean temperatures in this region. Helene developed and travelled over

water that was warming faster than the global average, increasing at a rate of 1.28°C per °C of global warming during.

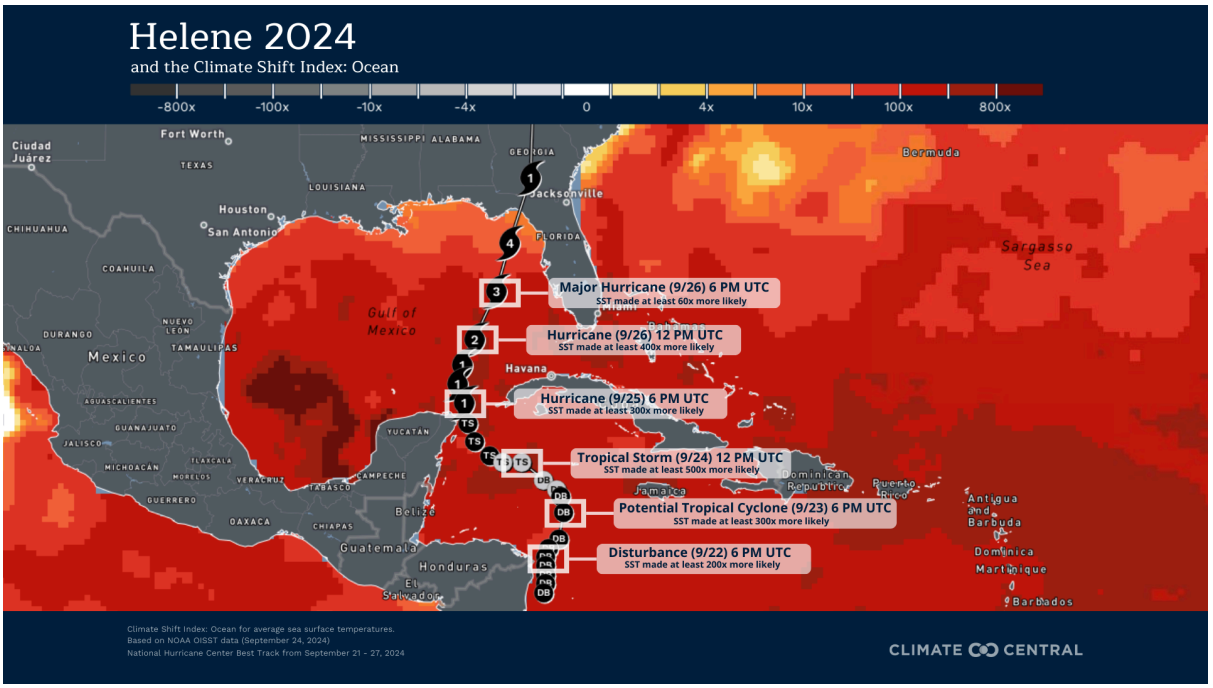

Figure 4.2:*Ocean CSI along the track of Helene, as it developed from disturbance to tropical storm to hurricane to major hurricane. Ocean CSI in surrounding regions are drawn from September 24th, when the storm developed from a potential tropical cyclone to a tropical storm, coinciding with the highest Ocean CSI (in excess of 500) measured along its track.*

4.3 Interpretation of results

Hurricanes intensities and rapid intensification are strongly related to elevated Sea Surface Temperatures (e.g. Hong and Wu 2021). Increased Sea Surface Temperatures allow for higher levels of local humidity, atmospheric instability, and potential intensity (e.g. Emanuel 2006). Along Helene's track, ocean temperatures were consistently more than 1°C warmer than they would have been in a world without climate change, and were made at least 200 times more likely during most of Helene's lifetime. We conclude that warmer Sea Surface Temperatures along the track of Hurricane Helene were strongly influenced by climate change, which affected Helene's environment and made it more likely for the storm to develop and intensify throughout its lifetime.

5 Wind speed attribution using IRIS

The event definitions studied in this section are as follows:

- **Florida landfall:** category 4 hurricanes making landfall in a region 2 degrees from Helene (figure 1.4)

Assessing tropical cyclone risk given the infrequency of landfalling tropical cyclones (TC) and the short period of reliable observations remains a challenge. Synthetic tropical cyclone datasets can help overcome these problems. We explore this method here using a new global tropical cyclone wind model (IRIS) with several key innovations. It recognises that the key step for estimating landfall wind speed is the location and value of the life-time maximum intensity (LMI). It redefines the problem as one of decay only. The initial intensity, life-time maximum, is assumed to be physically constrained by the thermodynamic state as defined by the potential intensity (PI).

5.1 Data and methods

Observations show that the relative intensity, defined as observed maximum intensity divided by the potential intensity, follows a robust uniform distribution. This drives the stochastic model lifetime maximum intensity. The landfall intensity is then a fraction of this lifetime maximum depending on the time to landfall. Tracks are based on IBTRACS observations. The original model description paper has been accepted for publication (Sparks and Toumi, 2024). IRIS calculates basin and landfall wind speed intensity distributions from the location of LMI and the corresponding potential intensity at that location, based on observed tracks between 1980 and 2024.

There has been a recent observed global warming of about 1.0°C, putting the global mean temperature close to about 1.3°C above pre-industrial temperature at the time of Gaemi. Regional and local prediction of absolute PI by climate models is problematic as they are known to have biases. Regional observed changes are difficult to distinguish from natural variability. We therefore make the assumption that the anthropogenic trend is the global zonal mean PI trend, and use the observed PI trend since 1979 from ERA-5 (figure 5.1). There is some warming from pre-industrial to 1979 for which we have incomplete potential intensity data. To estimate the pre-industrial potential intensity state we extrapolate backwards the current observed trends. This approach avoids the selection of any climate model. The method is simple and robust.

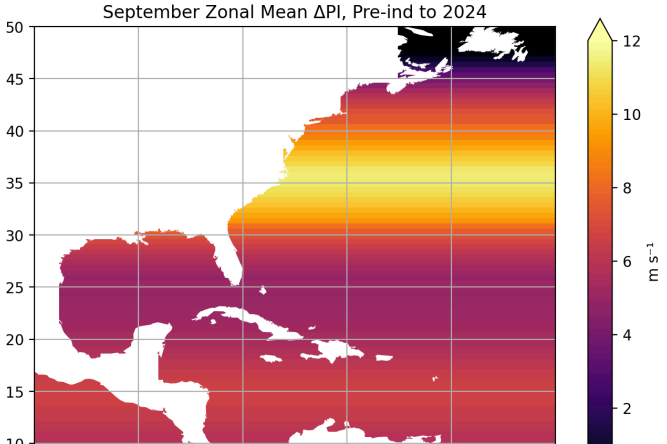

Figure 5.1: *Change in zonal mean potential intensity since pre-industrial conditions, based on the observed trend in ERA5 since 1979.*

5.2 Attribution

The change in wind speed for an event like Hurricane Helene striking the panhandle of Florida is clear. Such events now occur roughly once every 53 years, but prior to warming of 1.3 C would have occurred only once every 130 years. This represents an increase in likelihood of approximately 150%. Equivalently, events of a similar rarity to Helene in preindustrial times would have been approximately 6.1 m/s slower. This result is also in line with the observed change in PI over the Helene track shown in section 3.2.1 and summarised in section 6, which gave a change of +4.04 (1.79 - 6.15) m/s.

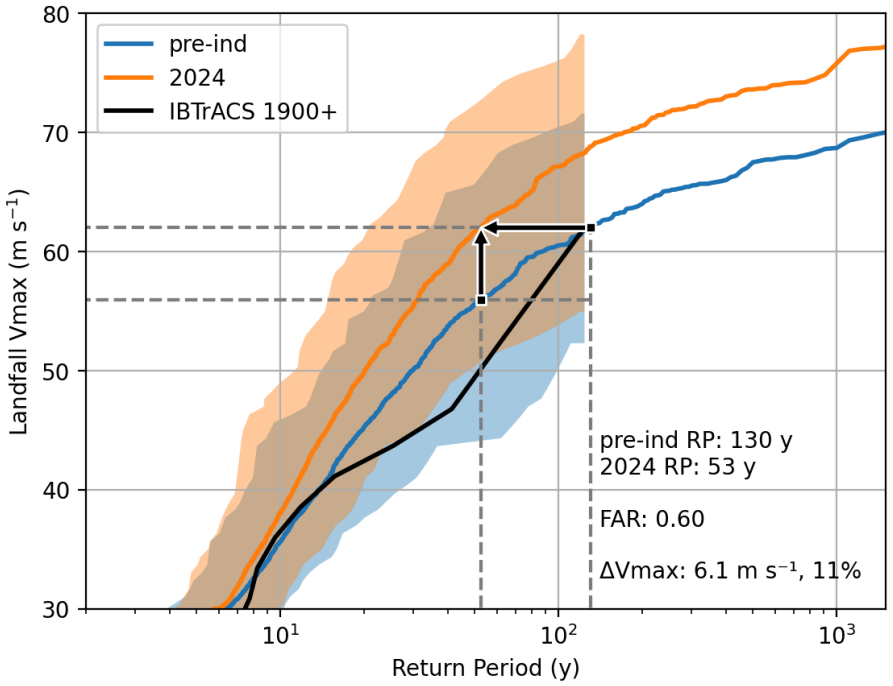

Figure 5.2: *Return curves for tropical cyclones making landfall around the same region as Helene. The orange curves show the present day climate in 2024, while the blue curves show the pre-industrial climate. The black line shows the distribution of observed storms in this region since 1980.*

5.3 Interpretation of results

This is a new approach, used in only one rapid study to date (World Weather Attribution, 2024), that sits alongside the usual WWA protocol. First, it is a single model, whereas WWA normally combines multiple models and approaches into a single statement. In general, additional models help to sample a wider range of possibilities to ensure that we are as close to reality as possible. However, this approach is fundamentally different in nature. It is a stochastic model that is not based on climate models, only on observations and well understood physics. This means that it is not subject to the same biases and challenges around simulating phenomena at small scales that climate models struggle with. Furthermore, it is based on a very large number of data points (~10000 years of synthetic data) and the results are tested against observed storm tracks and intensities.

With its basis in fairly simple and robust thermodynamic and physical arguments, this method is complementary to the WWA protocol. In particular, for tropical cyclones, it allows us to make statements about wind speeds that we cannot do on a rapid basis using the traditional method. This is because climate models (and therefore our method) are fundamentally limited in their ability to resolve the phenomena leading to these intensities. This approach just leverages other knowledge to bypass that challenge. However, overall, the results are still valid for the ‘class of event’ in the same way as our normal results, and thus the interpretation is essentially the same. Similarly, as shown by the study of storms close to the point of landfall, the analysis can be constrained in various ways so that they are as close to the impacts as we can manage.

6 Hazard summary

This section contains all of the final results for each hazard analysis.

While the return period of the rainfall depended heavily on the region, due in part to the different meteorological drivers of each, the synthesis results for influence of climate change on the extreme rainfall were very similar (tables 6.1 & 6.2). For both the coastal region around the panhandle of Florida and into southern Georgia, and the inland region around western North Carolina and eastern Tennessee, observations and models agreed that climate change from the preindustrial period to present has driven increases in likelihood and intensity of similar 2-day and 3-day extremes. Though none of the results were statistically significant, combining overall agreement with physical reasoning we conclude that climate change has amplified the amount of rainfall in both regions. The best estimates are as follows. In the coastal region, such rainfall now occurs roughly every 7 years, compared to 10 years previously, and is 10% more intense. In the inland region, such rainfall now occurs roughly every 70 years, compared to 116 years previously, and is 10% more intense. In the future at 2 C of warming, models project mostly statistically significant further increases in rainfall with respect to present. Coastal region extremes will become another 16% more likely and 3% more intense, while inland region extremes will become another 25% more likely and 3% more intense.

Changes in the potential intensity conditions forming such a storm are shown in table 6.2. Models and observations strongly agree on increases due to GMST, though observations give a much stronger trend to date. Synthesising both data sources, we find that such conditions have become significantly more likely at around a factor of 18 (3 - 142) and with a change in intensity of 4 (1.8-6.2) m/s. In future, models project a small non-significant increase, which is likely an underestimate.

However, the picture is much clearer for SSTs. According to the Ocean Climate Shift Index, anomalously warm SSTs similar to those along the storm track of Helene in September 2024 would have been extremely unlikely without global warming, with a rise of approximately 1 degree across the entire track, or equivalently an increase in likelihood of more than 200 in such conditions.

Finally, using IRIS, the wind speed of storms like Helene making landfall in the panhandle region of Florida have increased due to warming, becoming approximately 150% more likely (from a 130 year event down to a 53 year event) and about 6 m/s more intense.

Data		**Coastal region**		**Inland region**	
		Probability ratio (95% CI)	**Intensity change (%) (95% CI)**	**Probability ratio (95% CI)**	**Intensity change (%) (95% CI)**
Observations	**Past-Present**	2.13 (0.46 - 25.5)	21.5 (-23.4 - 92.5)	3.11 (0.47 - 63.1)	19.6 (-13.4 - 69.0)
Models		1.37 (0.78 - 2.52)	9.01 (-1.15 - 20.3)	1.51 (0.58 - 4.17)	8.49 (-2.72 - 21.1)
Synthesis		1.42 (0.83 - 2.58)	9.53 (-0.47 - 20.6)	1.66 (0.71 - 4.40)	9.52 (-1.24 - 21.6)
Models only	**Present-Future**	1.16 (1.07 - 1.27)	3.19 (1.52 - 4.79)	1.25 (0.99 - 1.60)	3.28 (1.62 - 4.92)

Table 6.1: *Summary of results for extreme precipitation in the coastal and inland regions, presented in Figs 2.5&2.6: changes due to GMST include past-present changes and present-future changes.*

Statistically significant increases (decreases) in probability and intensity are highlighted in dark blue (orange), while non-significant increases are highlighted in light blue (orange).

Data		**Potential intensity**	
		Probability ratio	**Change in intensity (m/s)**
Observations	**Past - present**	39.6 (1.82 - 5440)	4.26 (0.81 - 7.28)
Models		14.0 (1.54 - 132)	3.86 (0.90 - 6.80)
Synthesis		17.9 (2.85 - 142)	4.04 (1.79 - 6.15)
Models only	**Present - future**	1.93 (1.51 - 2.47)	2.02 (0.58 - 3.46)

Table 6.2: *Summary of results for potential intensity, presented in fig 3.2: changes due to GMST include past-present changes and present-future changes. Statistically significant increases (decreases) in probability and intensity are highlighted in dark blue (orange), while non-significant increases are highlighted in light blue (orange).*

Overall, it is clear that the rainfall, wind speeds and conditions leading to Hurricane Helene have all increased due to climate change. In particular, winds have become robustly more likely and intense, both regions of the US studied are experiencing more intense extreme rainfall and will continue to do so as the world warms further, and the warm sea surface temperature and potential intensity conditions leading to such an event will continue to become more intense.

It is therefore also overwhelmingly likely that the impacts of the hurricane were more severe as a result of climate change. These impacts were complex and occurred over multiple regions in different ways. Additionally, individual variables such as wind may drive impacts in different ways, such as through direct damage and driving storm surge, which may then compound rainfall-based flooding. In particular, while the changes in the magnitude of wind speeds seem small (~6 m/s), the damage potential of wind in the region of category 4 storms scales with the cube of intensity. Even small changes can therefore result in substantial increases in damage potential. In terms of this event, the impacts are also directly related to the multiple aspects of vulnerability and exposure of people affected by the storm (see section 7).

7 Vulnerability and exposure

In the days leading up to Hurricane Helene's landfall, a line of slow-moving showers formed along a stalled cold front, drawing in tropical moisture from Helene's outer edges. This system, stretching from Atlanta through the southern Appalachian region, saturated the ground and primed the southern states and Appalachia for the heavy rainfall that would accompany the hurricane.

Hurricane Helene made landfall in the southeastern U.S. on September 26, significantly affecting states such as Florida, Georgia, and the Carolinas. Coastal areas experienced severe wind damage, while inland regions, such as the southern Appalachians, were hit hardest by flash flooding. The steep terrain in these mountainous areas funneled rainwater into rivers and streams in the narrow valleys. In North Carolina, where more than half of the deaths occurred (Sutton et al., 2024), Buncombe County is estimated to be hardest-hit, including its main population center Asheville, as the French Broad River shattered previous records by 10 feet (over 3 meters), causing devastating flooding with water levels reaching rooftops in communities such as Swannanoa and Black Mountain (Davis, 2024). Counties adjacent to Buncombe are also heavily impacted, including rural populations of Avery, Mitchell and Tancey, as well as McDowell, Rutherford, Polk and Henderson counties.

While the full extent of Helene's impact will take months to fully assess, early reports show that Helene is the deadliest system to hit since Hurricane Katrina in 2005 with a staggering 232 fatalities to date (Sutton et al., 2024; ABC30, 2024). However, as highlighted by Young & Hisang (2024), mortality associated with tropical cyclones in the USA continues to rise years after the event itself. Economic disruptions, reduced access to healthcare, changes in social support networks, and environmental changes all play critical roles in this. Importantly, the hurricane has caused widespread damage and disruption to critical infrastructure and public amenities. Less than one-fifth of cellular sites were still down as of 6 October (FEMA, 2024), with over three million customers cut off from electricity in the Carolinas and Florida (Almasy, 2024; Yan & Almasy, 2024) and hundreds of roads including highways impassable (NYT, 2024), hampering emergency services and aid.

As of October 4th, major disaster declarations have been approved in 88 counties across Georgia, Tennessee, North Carolina and South Carolina. Many of these counties are ranked as moderately socially vulnerable by CDC's social vulnerability index, aligning with a large number of past disaster where socially vulnerable households have faced slower recovery and greater losses (Peacock et al., 2014; Zahran et al., 2008). CDC/ATSDR SVI indicators suggest that each of the 88 disaster declared counties were home to on average 30% of people below 150% poverty levels, 22.5% of housing cost burdened housing units, 29% minority population, 16% population with a disability and 6% population without vehicles. These figures suggest lower independent resources and capacity to prepare, respond and evacuate. Furthermore, on average, around 22% of housing units were mobile homes - a housing type that has been found to be highly vulnerable to losses (Rumbach, Sullivan, & Mackarewicz, 2020).

This rapid analysis delves into the underlying vulnerability and exposure dynamics that shaped Hurricane Helene's impacts, examining the factors that either amplified or mitigated the storm's destructive potential across affected regions. While further research and assessments on the ground

are essential to complement this study, it offers insights for improved flood risk management in a changing climate.

7.1 Flood risk

Historically, floods have more frequently affected western North Carolina (mountains and Piedmont) compared to the eastern portion of the state (coastal and tidewater) (Appalachian State University, 2019; Figure 5). Nevertheless, there were several western NC counties in lower elevations (between Asheville and Charlotte) with historically lower flood risks that were significantly impacted by Helene (First Street Foundation, 2021). In Georgia, historical flooding risk analysis has been focused on the state's coastal zones (between the state's borders with Florida and South Carolina), as counties in these areas have the greatest percentage area in flood risk zones (Binita et al., 2015). While Helene did pass through these coastal areas, the highest precipitation values were inland, with Atlanta and Augusta experiencing much of the storm's impacts. This disparity is similar for South Carolina, with the highest number of flood events historically affecting coastal South Carolina rather than the inland parts affected by Helene (PewTrust, 2016). In addition, the rapid urban development in South Carolina has significantly increased the risk of flash flooding, likely contributing to the impacts of a 2015 flash flooding event in the region (Cutter et al., 2017).

While coastal flooding related impacts are often a hazard associated with tropical storms, the prolonged precipitation associated with Helene caused significant pluvial and fluvial floods much further inland. In addition to the western most portions of North Carolina, several hardest hit areas in western South Carolina, northern Georgia and eastern Tennessee also are at moderate to very high risk of riverine flooding (FEMA Hazards, n.d.). Furthermore, the community resilience index, which measures the ability of a community to prepare for anticipated natural hazards, adapt to changing conditions, and withstand and recover rapidly from disruption, is low to moderate for these same areas (FEMA - Community Resilience, n.d.). When combined these two factors make the affected areas highly unprepared for a disaster such as Helene.

Although it is less common for flooding risks associated with tropical storms to affect areas so far inland, these flooding risks were not unfounded. A 2019 report titled 'Water is Coming' released by the Appalachian State University notes that the Great Flood of 1916 in Western North Carolina, which occurred when two heavy rainfall events occurred a week apart, is 'a notable example of how severe such inland flooding can be" including devastating impacts in Asheville and surrounding areas. (Appalachian State University, 2019). The NC climate report denotes that "heavy precipitation accompanying hurricanes that pass near or over North Carolina is very likely to increase, which would in turn increase the potential for freshwater flooding" (Kunkel et al., 2020).

It is possible that a lack of disaster memory and the lack of communication to the public of these increasing risks contributed to lack of preparedness in the affected areas. Situational factors such as proximity to a probable flood occurrence, degree of certainty that the hazard will occur, or homeownership status, as well as cognitive factors such as fear and worry are all cited as influencers of risk perception which is noted to vary greatly between the impacted areas, as exemplified by the distribution of flood insurance enrollment between the states which is estimated to be approximately 2x higher in Florida than in North Carolina (Lechowska, 2018, FEMA - Flood Insurance, 2024, NCDOI, n.d.). Additionally, focus group discussions held in northeastern US in 2020 revealed that

even individuals who have experienced detrimental impacts from previous floods perceive floods as a minor risk or concern compared to the other risks they are faced with in daily life, which may have led to less preparedness at the household level (Zinda et al., 2020).

7.2 Spatial planning and land-use changes

Spatial planning of built environments of communities can shape the degree of exposure to flooding in communities. By locating homes, businesses, offices outside flood-prone areas, and conserving natural habitats and ecosystems, planning can limit losses to people and assets. North Carolina has a tradition for high quality flood hazard mitigation planning (Lyles, Berke, & Smith, 2012). The Stormwater Service of City of Asheville NC regularly monitors runoff patterns on the French Broad River, and has installed green stormwater and stream restoration infrastructure to increase stormwater capacity (The City of Asheville, 2016). However, evidence also indicates gaps in moving the hazard mitigation plans to action (Horney et al., 2016) and ad hoc planning of interventions like buyouts hindering flood hazard mitigation (Siders, Hino, & Mach, 2019).

Under-regulated housing development in floodplains have contributed to exposure to flooding in North Carolina. Between 1996 to 2017, new housing development in North Carolina exceeded property buyouts or efforts to remove housing from floodplains by 10 to 1. Greater floodplain buyouts were seen in coastal communities compared to inland communities in North Carolina (Hino et al., 2023), suggesting a lack of buyout attention in inland North Carolinas in recent years.

The built environment of the western most portion of North Carolina also contributes to its economic vulnerability. When comparing the flooding hazard and exposure maps, the mountainous areas in the western portion of North Carolina tend to have higher exposure of property values within flood zones than counties in the Piedmont (central region) (Wang & Sebastian, 2021). Structural robustness of the built environment also plays a key part in exposure. Trailer and manufactured homes outside of Asheville, NC were severely impacted (Verduzco, Amy & Kruesi, 2024). This is part of a national pattern where certain housing types (e.g., manufactured homes) are associated with higher losses, due to a variety of factors including low-quality construction, location in highly floodplains, lack of alternative housing choices, and structural racism (Rumbach, Sullivan, & Mackarewicz, 2020; Nofal & van de Lindt, 2020; Fothergill & Peek; Horney et al., 2016).

Large scale agricultural activities are a huge part of the economy and livelihoods of the Southeastern US. Research has shown that aggressive agriculture expansion will amplify flooding hazards, while conversely, the land use change from pre-20th century widespread agricultural land to conservation and reforestation accounts for approximately 50% reductions in flood intensity over the region (Shen et al., 2024).

Moreover, spatial planning for flooding tends to focus on FEMA NFIP regulatory floodplains (Malecha, Woodruff, & Berke, 2021). The Pacific Northwest National Laboratory's Rapid Infrastructure Flood Tool (RIFT) estimations show that Hurricane Helene inundated neighborhoods beyond floodplains, eliciting the need for spatial planning beyond regulatory floodplains.

7.3 Flood risk management policy and insurance landscape

National Flood Insurance Program (NFIP) provides access to primary flood insurance policies which must be purchased separately since floods are not covered by homeowners insurance policies, transferring risk from homeowners to the federal government (Congressional Research Service, 2024). NFIP is also the policy responsible for the development and implementation of floodplain management standards meant to mitigate and reduce flood risk across the nation. NFIP engages in non-insurance activities such as flood hazard mapping (Flood Risk Information System, n.d.), disseminating flood risk information through flood maps (FEMA, n.d.-a), requiring community land use and building code standards (National Archives, 1979), and offering grants and incentive programs (FEMA, n.d.-b) for household and community level investments with a long term goal of reducing federal expenditure on disaster assistance after floods. Over 22,000 communities across the United States participate in NFIP (FEMA, 2024).

Despite the known benefits of flood insurance there is a large insurance gap in the U.S., with an estimated 30% of homeowners in the southern region having flood insurance in 2020, increased from 16% in 2018, possibly due to mortgage lender requirements for flood insurance in special flood hazard areas, according to a poll by the Insurance Information Institute (Insurance Information Institute, 2021). However, this number is self-reported and actual coverage is likely much lower. For example, in 2019 the North Carolina Department of Insurance estimated that less than 3% of properties had flood insurance coverage through the NFIP (NCDOI, n.d.). The coverage gap may be worse in inland communities than the overall region due to a perception of lower flood risk (APPSTATE R.I.S.E, 2019). One estimate using U.S. Census occupancy estimates and NFIP policy data predicted North Carolina single-family dwelling homeowners may be insured at a rate as low as 5 percent in some municipalities (APPSTATE R.I.S.E, 2019) and Keys and Mulder (2024) note that flood insurance throughout the United States is largely purchased by homes in floodplains despite clear evidence that flood risk is more widespread (First Street Foundation, 2020). Consumer knowledge of the insurance industry, ability to pay for optional flood insurance coverage, and distrust in the institutions surrounding flood insurance are additional reasons cited for low enrollment in flood insurance plans in the United States (Kousky & Netusil, 2023; Netusil et al, 2021; Zinda et al, 2021).

The Florida State Floodplain Management Program (2015) launched a pilot initiative from 2015-2017 called CRS-CAV to promote participation in FEMA's Community Rating System (Flood Science Center, n.d.-a), which offers discounts on flood insurance premiums for communities that adopt enhanced floodplain management practices. Florida also requires local permits for any land-disturbing activities in flood zones. Undeveloped coastal barriers are ineligible for flood insurance under NFIP (Flood Science Center, n.d.-a) so Florida restricts development in coastal areas through its Coastal Construction Control Line program (Flood Science Center, n.d.-b).

The State of Georgia entered into a Cooperating Technical Partner agreement with FEMA in 1999 to assume responsibility for developing and updating flood hazard maps for all 159 counties in the state (Environmental Protection Division, n.d.), allowing for efficient use of public funds and better alignment of flood mapping with Georgia-specific needs (FEMA, n.d.-c). There are 71 communities in Georgia with mapped special flood hazard areas that are not participating in NFIP (Environmental Protection Division, n.d.).

North Carolina has developed the Flood Risk Information System (2017), which allows users to assess their flood hazard vulnerabilities and consider mitigation options associated with known flood

risks. Like Georgia, NC also has a cooperating technical partner agreement with FEMA and, similar to Florida, NC encourages communities to participate in FEMA's community rating system. Uniquely, North Carolina adopted a policy in 2022 that updated design and construction requirements for state government and university buildings in flood-prone areas (Department of Administration, 2024). Key components of the policy include increasing elevation requirements for construction in coastal areas and preventing construction of state-owned buildings in 100-year and 500-year floodplains.

Tennessee operates a State Floodplain Management Program (TN Association of Floodplain Management, 2024), which serves as the State Coordinating Agency for the NFIP, but also an advocacy and awareness tool for flood risk.

There is limited research available on the policies and programs that have been proposed yet ultimately rejected in the affected states, regions, or communities that may have reduced overall impact had they been implemented.

7.4 Flood protection infrastructure

Hurricane Helene made landfall near Perry, Florida and had a storm surge between 6 and 15 feet (NHC Storm Surge). Florida's Big Bend region depends on natural floodplains rather than an extensive levee system or flood barrier, increasing the importance of evacuations in low-lying areas near the coast. The sparse population of this part of Florida likely helped to limit impacts. Despite making landfall over 100 miles away, storm surge in Pinellas county and the densely populated Tampa Bay area inundated homes, businesses and roadways and tested green infrastructure projects implemented in this region (Pinellas, 2024).

Across North Carolina, Georgia, Tennessee and Florida, the intense rainfall from the hurricane overwhelmed drainage systems and resulted in widespread power outages and road closures. Along the path of Hurricane Helene, in the southeastern US and up to North Carolina there is a network of dams, and drainage systems intended for different water management purposes such as providing water during drought times and protecting people from floods during periods of extreme rainfall. About 25% of all critical infrastructure in the US is at risk of becoming inoperable due to flood risks (First Street, 2023). In North Carolina where the majority of deaths occurred, 1372 of the total 3533 dams are classified by the US Army Corps of Engineers as highly exposed to hazards and having a fair, poor or unsatisfactory condition (USACE). This is characteristic of the aging water infrastructure across the southeastern US (Amado & Liu, 2023). Another side to the problems is that across the world, existing flood defense infrastructures are becoming inadequate to meet the climate change-induced escalating flood risks we face today (Griffis, 2007; Kelley, 2019; Kreibich et al., 2015).

Following the extreme rainfall from Helene several dams were at risk of critical failure including the Walters and Lake Lure dams in North Carolina (GuyCarp, 2024). At the Lake Lure Dam in North Carolina thousands of people were evacuated downstream and the water overtopping the dam caused erosion on one side, although it ultimately avoided failure (Wolfe, 2024). Rising water levels rendered Nolichucky Dam in Tennessee, and the Waterville Dam in North Carolina at risk of imminent failure (Lacey, 2024; Yoon, 2024). While, as of the writing of this report, a dam failure ultimately did not occur, the possibility of dam breaches did catalyze evacuation from downstream communities including from Unicoi County Hospital (Dodds, 2024; Yoon, 2024). The US Army Corps of

Engineers was closely monitoring several dams prior to the storm and they largely functioned as engineered, with spillways used to release excess water when needed (USACE Nashville District, 2024). Current flood protection infrastructure did not account for heavy rain cascading into landslides and mudslides in mountainous regions leading to the destruction of homes, businesses and roads (Washington Post, 2024).

7.5 Early warning early action

The United States has a robust early warning system for hurricanes run by the National Weather Service including a National Hurricane Center that monitors hurricane formation throughout the Atlantic, Caribbean Sea and Gulf of Mexico, as well as the Central and Eastern Northern Pacific (National Weather Service, n.d.; National Hurricane Center, n.d.).

The National Weather Service and the National Hurricane Center began issuing alerts about Hurricane Helene on September 23rd, 2024 (NOAA-NHC, 2024). On September 25th, predictions from NOAA's National Water Centre's 7-day Flood Hazard Outlook for Western North Carolina went from 'considerable' to 'catastrophic' by 3pmEST (NOAA-NWC, 2024). On the same day, NOAA issued a rare press release further emphasizing the urgent need for inland communities to prepare for life-threatening flooding, citing locations such as Western North Carolina, including Asheville. This release included a top-line directive, in red, with italicized font for further emphasis, stating: "*Reporters: This is a rare news release from NOAA for an operational weather event. We urge the news media to continue focusing the public's attention on the major impacts from inland flooding expected along the path of Helene well after landfall* (NOAA, 2024).

Governors declared a State of Emergency in advance of Hurricane Helene on September 23rd, 2024 in Florida (State of Florida, 2024a); September 24th in Georgia (State of Georgia, 2024a); September 25th in North Carolina, South Carolina and Virginia (State of North Carolina, 2024a), State of South Carolina, 2024, State of Virginia, 2024) and September 26th in West Virginia (State of West Virginia, 2024).

Various county, city and town executives also declared local State of Emergencies following the gubernatorial declarations, for example the cities of Tampa, Florida (City of Tampa, 2024) and Bonita Springs, Florida (City of Bonita Springs, 2024), Murphy, North Carolina (Town of Murphy, 2024) and Hendersonville, North Carolina (City of Hendersonville, 2024). As well as various counties in North Carolina, including the ultimately hard-hit counties of Avery, Buncombe, McDowell and Mitchell (WLOS, 2024). This mechanism allows authorities to mobilize human and financial response resources in advance of the Hurricane's landfall to reduce potential impacts. In North Carolina, for example, authorities pre-positioned 19 swift water rescue teams and activated three urban search and rescue task forces (WRAL, 2024).

In advance of Helene's landfall the federal government pre-staged "more than 2.7 million meals, 1.6 million liters of water, 50,000 tarps, 10,000 cots, and 20,000 blankets in the region to support sheltering needs in impacted communities." FEMA also sourced hundreds of ambulances for patient needs and pre-positioned more than 70,000 gallons of diesel fuel and more than 40,000 gallons of gasoline to reduce potential fuel shortage. The Department of Housing and Urban Development

“notified Public Housing Authorities, multifamily, and healthcare facility owners to implement all appropriate protocols to prepare for the storm and ensure the safety of their residents” (White House, 2024). The American Red Cross mobilized 400 disaster responders and stocked 45,000 snacks and ready-to-eat meals to support immediate needs (C. Housman, October 3, 2024).

By September 25th, voluntary and mandatory evacuation orders were in effect across multiple counties in Florida and Southern Georgia, and September 27th in North Carolina. Overnight shelters were opened to facilitate evacuation (State of Florida, 2024b; WTXL, 2024; WXII, 2024). Evacuation alerts were also sent directly to cell phones via FEMA’s Integrated Public Alerts and Warning System as the storm approached and news outlets were regularly reporting on safety and preparedness measures in the Helene’s projected path.

Despite the accuracy of predictions, and as the Associated Press described ‘an all out-blitz’ by the National Weather Service to warn people in its impending path days in advance, many in the worst affected regions of North Carolina were still caught off guard (AP, 2024a). Full after action reviews will be necessary to understand what could have gone better, if anything. Initial reporting indicates that despite alert messages being sent, spotty cell and internet reception in the mountainous areas means that messages did not always go through, other reports indicate that local alert messages may have been sent too late - after flood waters were already rising (Citizen Times, 2024). Some residents had never experienced a Hurricane before, while others who had experienced flooding assumed it would not be so bad if not in a valley (AP, 2024a). Although 7% of Buncombe county residents are Hispanic or Latino no emergency phone alerts were sent in Spanish (Washington Post, 2024b) though alerts were posted in Spanish on Facebook (Citizen Times, 2024). Evacuation orders were also voluntary rather than mandatory (NYT, 2024). At the same time, the timing of evacuations is important in the mountainous regions people could have been stuck on roads and that could have been more disastrous, routes out of many communities are not labeled, and even if they were, the difficult mountain terrain often means one-road in and out of small towns (Washington Post, 2024b). Lessons from other Hurricanes also shed light on the complexity of disaster evacuations (AJPH, 2011).

7.6 Emergency response

Following Helene’s landfall, Major Disaster Declarations were approved by the President of the United States on September 29th for Florida and North Carolina, September 30th for South Carolina, October 1st for Georgia and October 2nd for Tennessee and Virginia (FEMA, 2024a; FEMA, 2024b; FEMA, 2024c; FEMA, 2024d; FEMA, 2024e; FEMA, 2024f). Additional states of emergency declarations were issued or extended at local levels, for example, Atlanta, Georgia; Augusta, Georgia; and Tampa, Florida, among others (City of Atlanta, 2024; WGAC, 2024; City of Tampa, 2024).

By September 27th, 940 Urban Search and Rescue personnel were deployed to affected states, many before the storm’s landfall, along with 1,500 federal personnel (White House, 2024a). These numbers grew to over 1,250 and over 4,800 by October 2nd (White House, 2024c). Also by September 27th, National Oceanic and Atmospheric Administration (NOAA) experts were deployed to gather aerial footage of storm damage and assess key waterways to reopen transport routes. The State of Florida also requested and had approved operational flexibility to deliver the State’s school lunch program during school closures (NOAA, 2024a; White House, 2024).

By September 29th over 50,000 personnel from 31 States, the District of Columbia and Canada were deployed to respond to power outages which peaked at 4.6 million people without power on September 27th (White House, 2024b). By October 2nd, 1.6 million people remained without power and FEMA had deployed over 50 Starlink Satellites to support disaster communications (White House, 2024c). The Federal Aviation Administration deployed satellite communications kits to Asheville Airport to restore airport operations (USDOT, 2024). The US Department of Health and Human Security (HSS) deployed emergency support teams to provide surge capacity at local hospitals and mortuaries (White House, 2024c).

By September 29th, over 6,300 National Guard members were mobilized from 12 states to support emergency operations across six states including search and rescue and clearing debris from thousands of miles of roads (US Army, 2024). On October 2nd, an additional 1,000 active-duty soldiers were deployed to North Carolina on request of the Governor, to supplement national guard and local emergency responder efforts (State of North Carolina, 2024b).

The City of Asheville, North Carolina, one of the hardest hit areas, issued boil water advisories, suspended public transport services, announced curfews, launched water distribution sites and held response briefings two times a day over Facebook and FM radio to share updated information with residence such as the locations of new temporary cell towers (City of Asheville, 2024).

Complicating response efforts in Western North Carolina is the mountainous and relatively remote terrain, where many smaller towns and communities remained cut-off as of October 2nd, with critical supplies being airlifted to affected populations and in some cases brought in by mules and on foot (State of North Carolina, 2024c; NBC, 2024; BPR, 2024).

In addition, potable water access was severely disrupted with water treatment facilities, water main lines and distribution networks damaged and/or destroyed due to the floods. Water tankers were brought in as a stop-gap measure with disrupted cell systems, already spotty before the storm, complicating messaging about water access points (Washington Post, 2024). In rural areas, residents rely on wells and/or septic systems for drinking water and sanitation which are also prone to contamination during floods and will need individual testing and treatment before they are considered restored (NCDHHS, 2021, NCDHHS, 2024).

A variety of Voluntary Organizations Active in Disaster's (VOAD) 79 national member organizations are also providing relief (VOAD, n.d.). For example, as of October 3, the American Red Cross has 1,500 workers supporting relief efforts and has provided 100,000 meals and snacks. In addition, more than 200 Red Cross staff are working on some 4,000 family reunification requests – with more anticipated in the days ahead. (C. Housman, October 3, 2024) World Central Kitchen[1] has partnered with restaurants and food trucks across Florida, North Carolina, Tennessee, and Georgia to distribute hot meals. They have also delivered tanker trucks full of water (World Central Kitchen, 2024). The Humane Society was active in Florida and Tennessee providing shelter, supplies and veterinary services for pets (Humane Society, 2024). Feeding America deployed 42 truck loads of food, water and relief supplies to 11 local food banks in the Southeast (Feeding America, 2024). Samaritan's Purse deployed an emergency water filtration system with capacity to serve 10,000 people a day, and

[1] Not a VOAD member

an emergency field hospital extending local emergency room capacity (Samaritan's Purse, 2024a Samaritan's Purse, 2024b) and Habitat for Humanity was assessing Hurricane Helen damage to be ready for long term recovery; among other organizations (Habitat for Humanity, 2024).

Community resources were also created by local volunteers to assist with locating supplies, though individuals who remain disconnected from cell service and/or wifi or unable to connect with social support may be unable to access these digital resources (Google Sheet, 2024; Google Doc, 2024).

7.7 Government social protection systems

A variety of social protection programs are activated alongside a Major Disaster Declaration.

The Federal Emergency Management Administration (FEMA) runs an Individuals and Households Assistance Program (FEMA, 2024a) where disaster affected individuals can apply for: rental assistance, lodging expenses, home repair, immediate needs (water, food, prescriptions, personal hygiene, diapers etc), personal property (appliances, furniture, uniforms etc), medical/dental care, childcare, transportation, moving and storage expenses. FEMA also operates the Disaster Legal Services program, providing free legal aid to disaster survivors in partnership with the American Bar Association (FEMA, 2024b).

As of October 2nd, 2024, Disaster Unemployment Assistance (DUA) program was activated for 25 counties and the Eastern Band of Charokee Indians in North Carolina, 11 counties in Georgia, 13 counties in South Carolina, and 22 counties in Florida (USDOL, 2024; State of North Carolina, 2024d; State of Georgia, 2024b; SCDEW, 2024; State of Florida 2024c). On October 3rd, six counties and one city in Virginia and eight counties in Tennessee were added (WAVY, 2024; State of Tennessee, 2024). DUA is a federal program under the US Department of Labor that provides unemployment benefits for up to 26 weeks for employed and self-employed individuals whose employment is lost or interrupted due to a major disaster.

The US Department of Agriculture (USDA) Food and Nutrition Service (FNS) operates the Supplemental Nutrition Assistance Program (SNAP) providing food benefits to low-income families via funds transfer to an Electronic Benefits Transfer (EBT) card (USDA-FNS, 2024a). Following a Major Disaster Declaration, this program can be scaled-up and out via D-SNAP, the Disaster Supplemental Nutrition Assistance Program, if assistance is requested by state authorities and approved by USDA. Under D-SNAP, existing SNAP beneficiaries can apply for supplemental assistance, and those who would not normally meet income qualifications for SNAP can qualify for an EBT card if they have incurred disaster losses (USA, 2024). The Food and Nutrition Service also oversees the National School Lunch Program (NSLP), along with a variety of other Child Nutrition Programs. The NSLP which offers reduced cost lunches to children that meet certain requirements such as income levels or based on their status such as homeless, migrant, runaway, or foster children. (USDA-FNS, 2017) During disasters USDA-FNS can approve state requests to waive certain program criteria such as the hours food is served or the location etc. As of October 4th 2024, USDA-FNS had approved a variety of measures related to Child Nutrition Programs and SNAP benefits in Florida, Georgia, North Carolina, South Carolina, Tennessee and Virginia (USDA-FNS 2024c, USDA-FNS 2024d, USDA-FNS 2024e, USDA-FNS 2024f, USDA-FNS 2024g, USDA-FNS 2024h).

The US Small Business Administration activated its Physical Damage Loan program, available to homeowners, renters, nonprofits and businesses, it covers losses not covered by insurance (USSBA, 2024a; USSBA, 2024b). This loan does not cover property upgrades, but there is a complimentary Mitigation Assistance program where loan applicants can request an additional 20% for property enhancements that mitigate future disaster risks (USSBA, 2024c). An additional program is the Economic Injury Disaster Loan, available to small businesses, small agriculture cooperatives and nonprofits, it covers running costs such as utilities, health care benefits, fixed loan repayments etc. (USSBA, 2024d). The goal of this loan program is to help small businesses survive and recover from disasters. Both of these loan programs have fixed, low interest rates (ranging 4-8%) with up-to 30-year repayment schedules.

The Substance Abuse and Mental Health Services Administration (SAMHSA) operates a Disaster Distress Helpline for disaster-related counseling services (SAMHSA, 2024). On October 2nd 2024 the Centers for Medicare and Medicaid (CMS) activated emergency accelerated and advance payments to medical providers, as well as debt restructuring options for providers on debt repayment plans. Both efforts aim to ensure adequate cash-flow at medical facilities responding to client needs (CMS, 2024).

On September 30th and October 1st 2024, authorities issued moratoriums in Florida, Georgia, North Carolina, and South Carolina to preventing insurers from canceling casualty policies due to non-payment after Helene (FLOIR 2024, OCI 2024, NCDOI 2024, SCDOI 2024). In Tennessee authorities have requested a moratorium be executed (FMCSA 2024). Also on October 1st, the Internal Revenue Service (IRS) issued tax payment extensions, allowing individuals and businesses in affected areas to postpone tax filings and payments until May 1, 2025, including quarterly income payments, payroll taxes and excise taxes (IRS 2024).

Finally, the USDA Farm Services Administration (FSA) may also provide special assistance to farmers, ranchers and orchardists via a suite of programs that can be activated following a Major Disaster Declaration, these include: Emergency Farm Loans, the Emergency Conservation Program, Farm Operating Loans, the Livestock Indemnity Program, the Noninsured Crop Disaster Assistance Program, the Tree Assistance Program, the Emergency Forest Restoration Program and the Emergency Assistance for Livestock, Honey Bees, and Farm-raised Fish (USDA-FSA, n.d.-a; (USDA-FSA, n.d.-b; USDA-FSA, n.d.-c; USDA-FSA, n.d.-d; USDA-FSA, n.d.-e; USDA-FSA, n.d-f; USDA-FSA, n.d.-g; USDA-FSA, n.d.-h; USDA-FSA, n.d.-i), as well as additional non-disaster programs that remain relevant in times of disaster, such as the Single Family Housing Guaranteed Loan Program for elderly or very low-income applicants (USDA-RU, n.d.).

7.8 Compounding event and cascading impacts

Tropical Cyclone Fred in 2021 had an analogous track to Helene, with some similarities in impacts. For example, Fred resulted in record-breaking rainfall in western North Carolina, washing away roads and bridges, swelling local rivers and resulting in mudslides (Tropical Storm Fred Public Action Plan, 2023. As of January 2023, 13.186 million has been allocated for disaster recovery needs, especially yet unmet housing and infrastructure needs, and people and infrastructure had not fully recovered by the time Hurricane Helene came through (Tropical Storm Fred Public Action Plan, 2023).

High temperatures may have significantly exacerbated the vulnerabilities of individuals affected by the flooding associated with Hurricane Helene. According to Occupational Safety and Health Administration (OSHA) guidelines (UCMERCED, 2021), temperatures exceeding 80℉ increase the risk of heat-related illness, particularly during strenuous physical labor, such as post-hurricane search and rescue, clean-up, and reconstruction. Following the hurricane, many individuals were left without power, limiting access to cooling systems and increasing the exposure to dangerous heat levels. Figure 7.1 presents a geographic distribution of the number of days with temperatures exceeding 80℉ by county, accompanied with data on power outages following Hurricane Helene. The darker hues represent regions experiencing more days of high temperatures, primarily concentrated in southern states like Florida and Georgia. Black circles in the map indicate counties that experienced power outages, with the highest density of outages observed in areas with higher temperatures. The lack of reliable access to clean water further compounded the risks, as hydration is also essential for preventing heat stress.

Additionally, the temperature threshold of 80℉ does not take into account the role of humidity, which an significantly increase heat stress. After Hurricane Helene made landfall in Florida, many areas were placed under heat advisories, with heat indices ranging from the high 90s to low 100s, even though ambient temperatures were around 80℉. These heat indices represent a more accurate measure of how hot conditions feel to the human body when accounting for humidity, which significantly intensified the potential for heat-related illnesses.

In the absence of power and water, what might seem like moderate temperatures under normal conditions became dangerous, particularly for vulnerable populations engaged in physically demanding tasks. This combination of heat, humidity, power outages, and water disruptions amplified the health risks in the aftermath of the hurricane, worsening the already precarious situation.

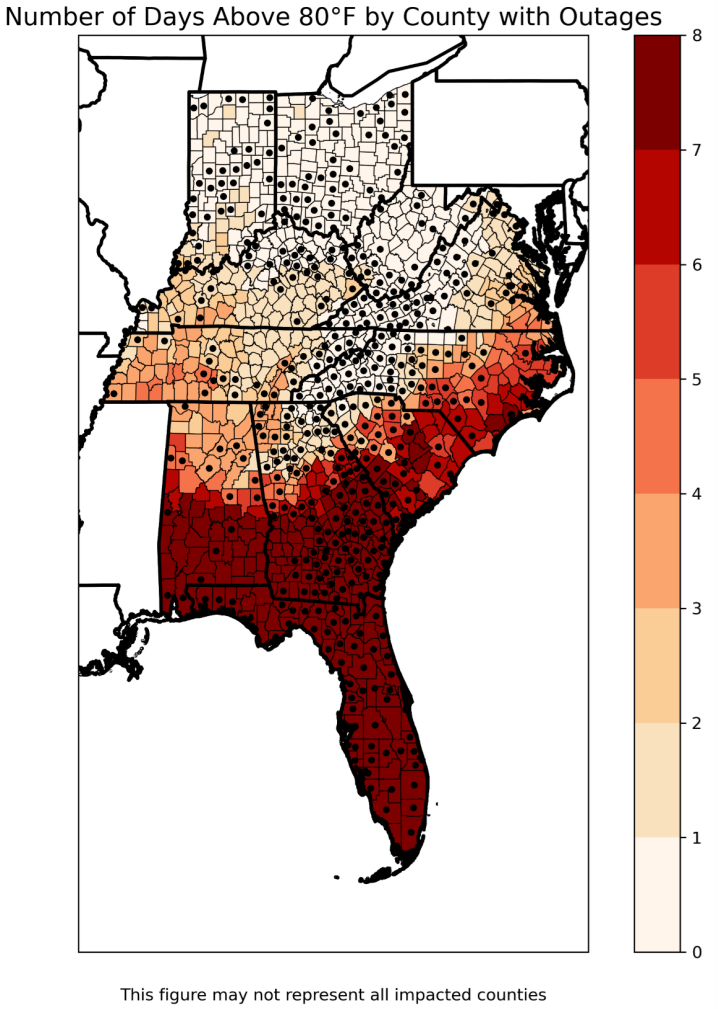

Figure 7.1. *Number of days above 80℉ by County with outages. Source: Climate Central. Temperature data was sourced from ERA5, and power outage data was obtained from the USA Today power outage tracker, which aggregates data from multiple utility companies.*

V&E Conclusions

This rapid analysis of vulnerability and exposure factors related to Hurricane Helene reveals a combination of policies, planning, infrastructure and response intended to reduce impacts from the extreme rainfall that hurricanes produce. This includes proactive spatial planning in states like North Carolina that accounts for floodplains, an increase in the flood insurance enrollment, comprehensive social safety net programmes and highly accurate early warnings. Yet, while each of these protections exist, there remain issues in implementation. For example, buyouts and spatial planning interventions have been largely ad hoc, without comprehensive or strategic implementation in the places where it's most needed. While flood insurance is available, the process of obtaining it remains complex and expensive for many Americans. While there was no dam failure resulting from the extreme rainfall, other forms of critical infrastructure that are required for recovery after the storm (e.g. roads, potable water, electricity, telecommunications, healthcare, etc.) were severely damaged. Early warning systems adequately conveyed the likely storm track and risk of inland flooding, but it is not clear to what extent the populations in the highest risk areas understood and heeded the warning. The extreme

nature of the event, combined with the unusual (but not unprecedented) inland floods exploited these deficiencies in the existing policies and planning resulting in devastating impacts.

Data availability

All time series used in the attribution analysis are available via the Climate Explorer.

References

All references are given as hyperlinks in the text.

Appendix

A.1 Model evaluation figures

A.1.1 Extreme rainfall

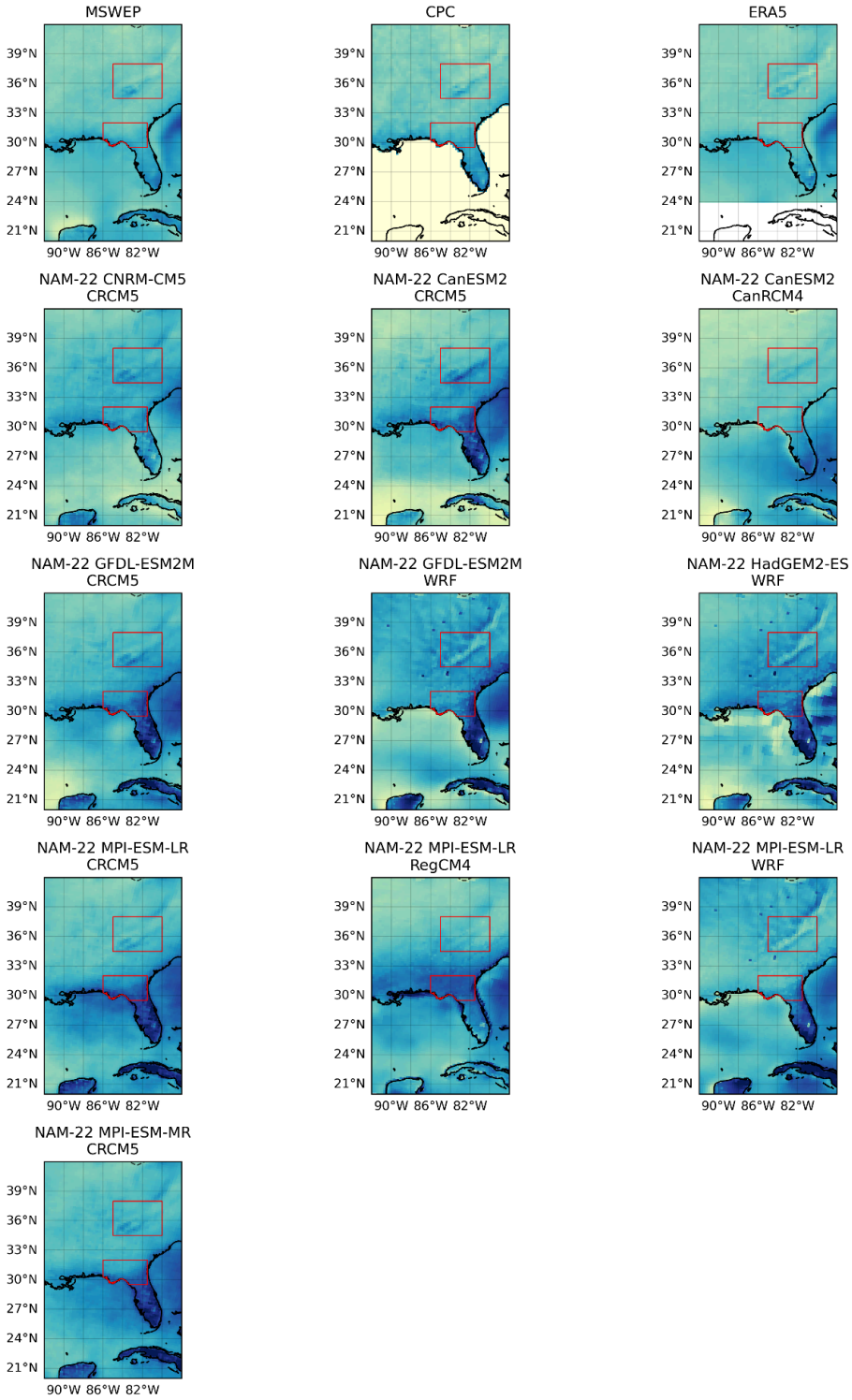

Figure A.1: *Spatial patterns of precipitation in June-November in observations and CORDEX models. The two study regions for the rainfall analysis are highlighted in red.*

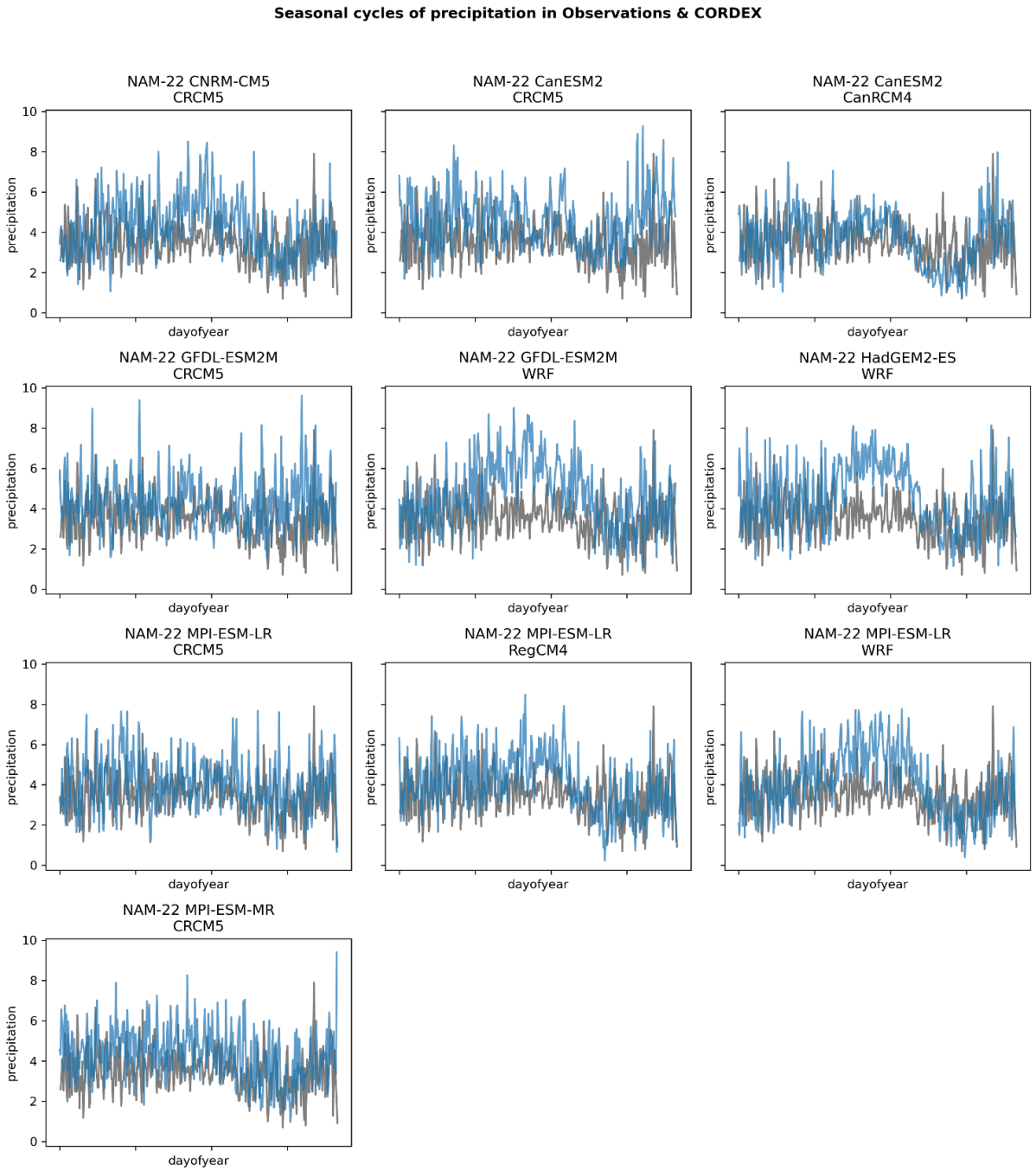

Figure A.2: *Seasonal cycles of precipitation in the inland region in observations and CORDEX models.*

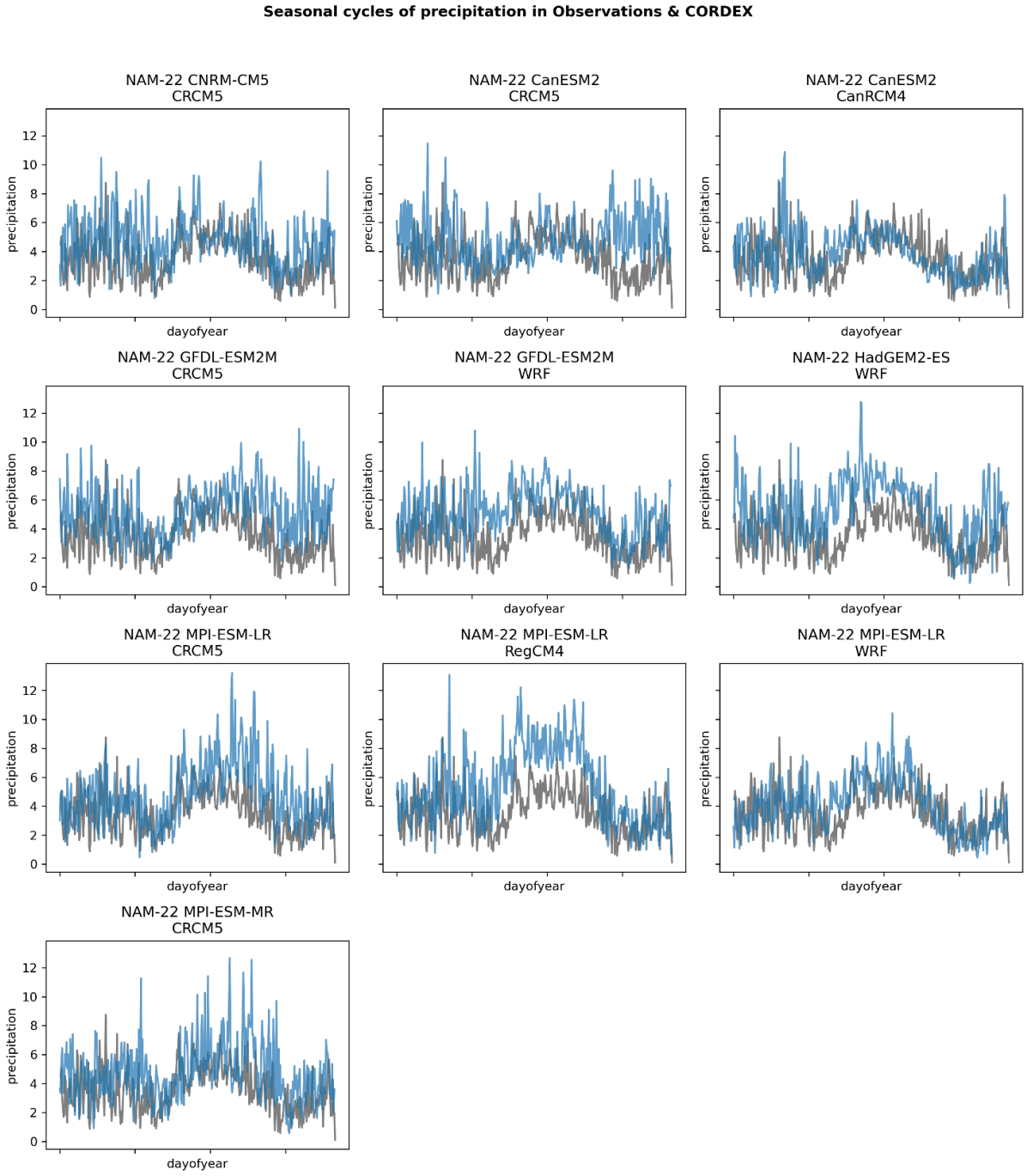

Figure A.3: *Seasonal cycles of precipitation in the coastal region in observations and CORDEX models.*

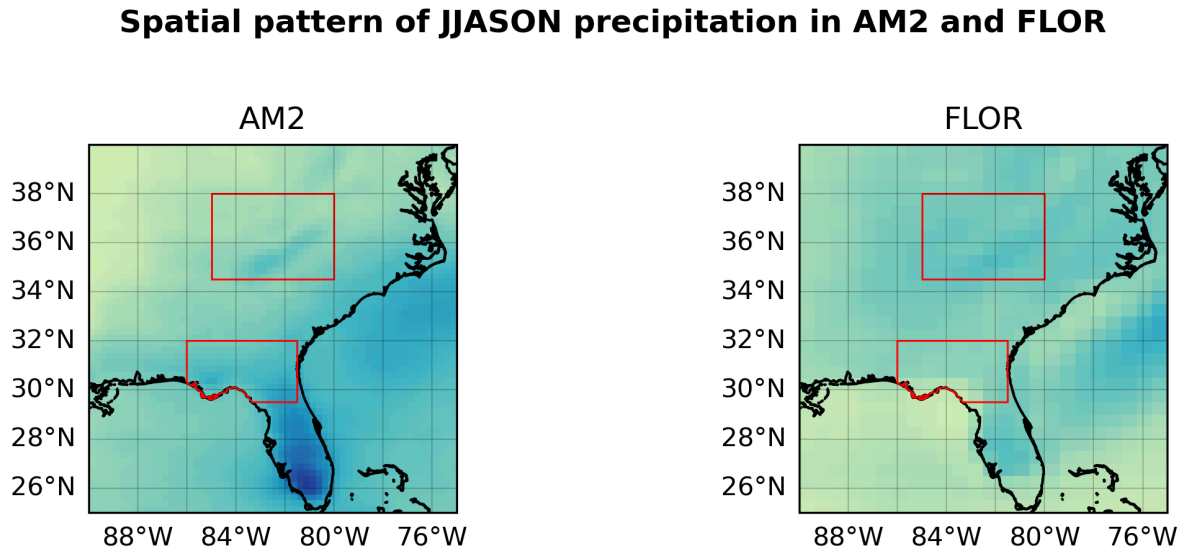

Figure A.4: *Spatial patterns of precipitation in June-November in observations and AM2 and FLOR models. The two study regions for the rainfall analysis are highlighted in red.*

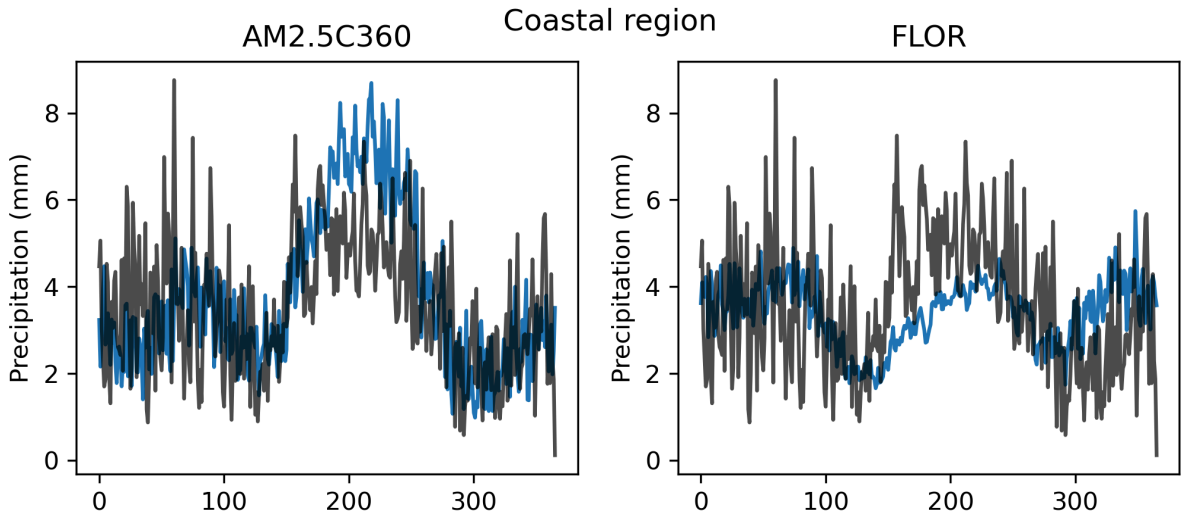

Figure A.5: *Seasonal cycles of precipitation in the coastal region in observations and AM2 and FLOR models.*

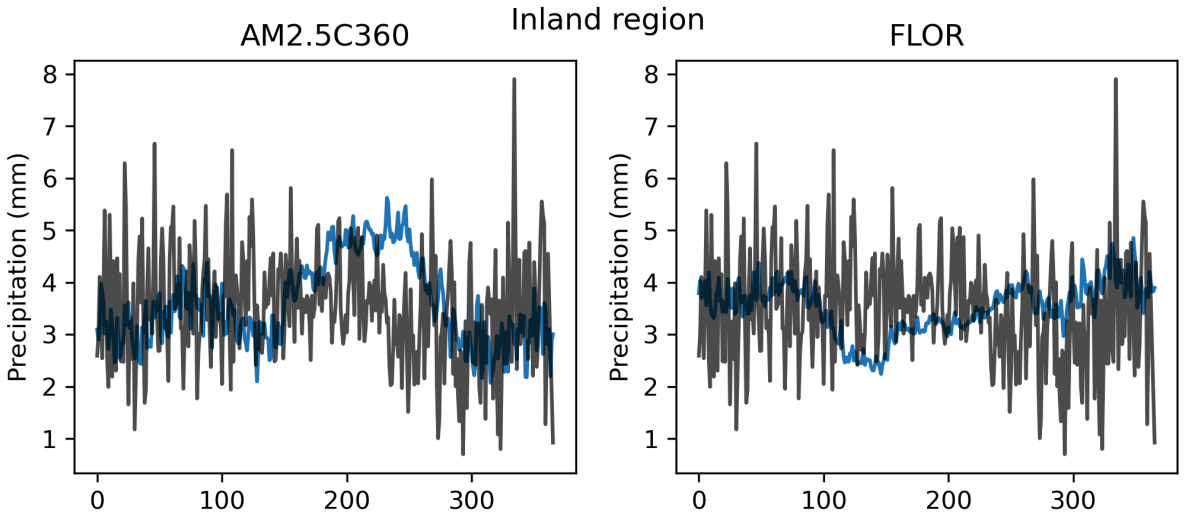

Figure A.6: *Seasonal cycles of precipitation in the inland region in observations and AM2 and FLOR models.*

A.1.2 Potential Intensity

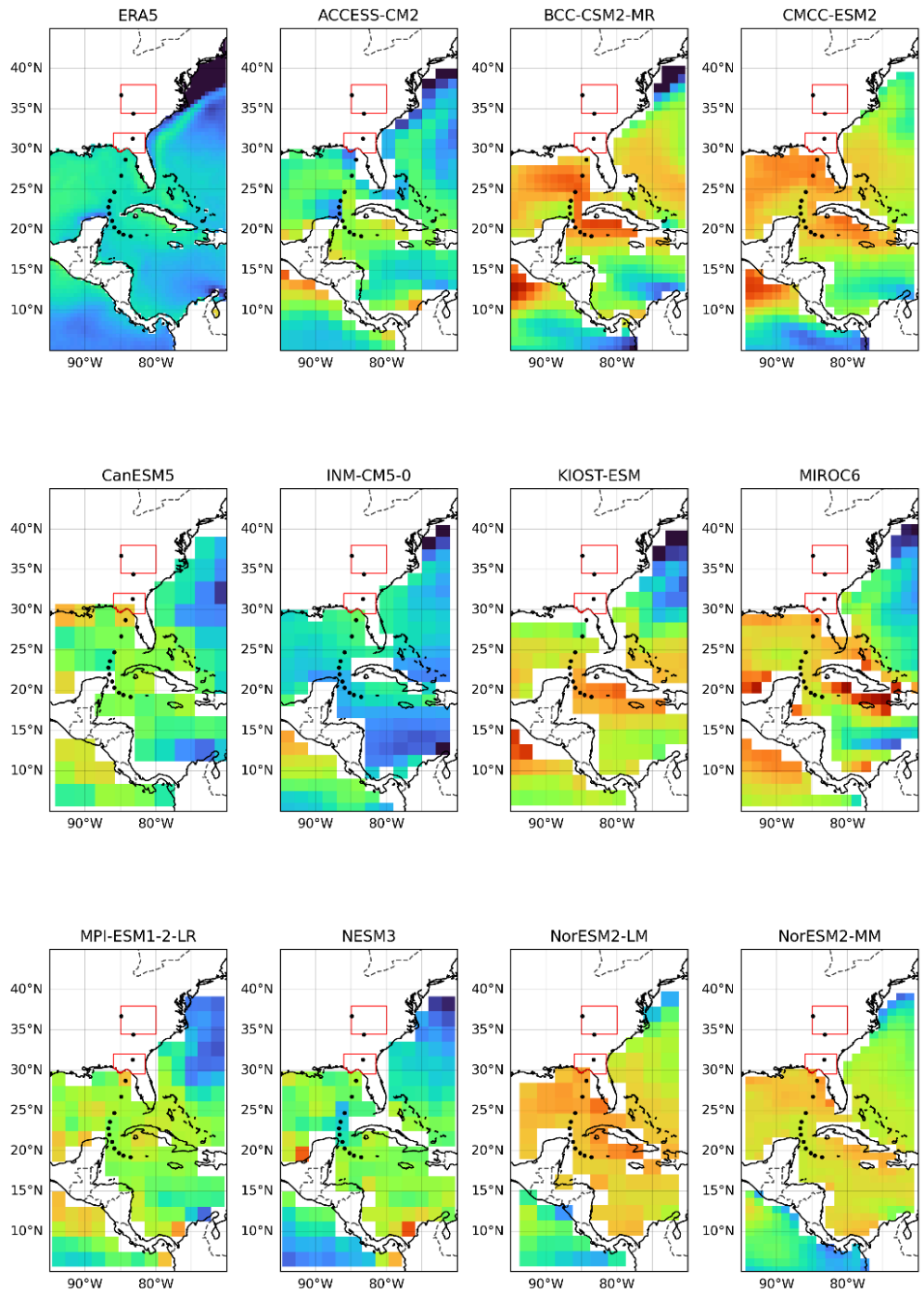

Figure A.7: *Spatial patterns of potential intensity in September in ERA5 and CMIP6. The two study regions for the rainfall analysis are highlighted in red and track of Helene in black.*

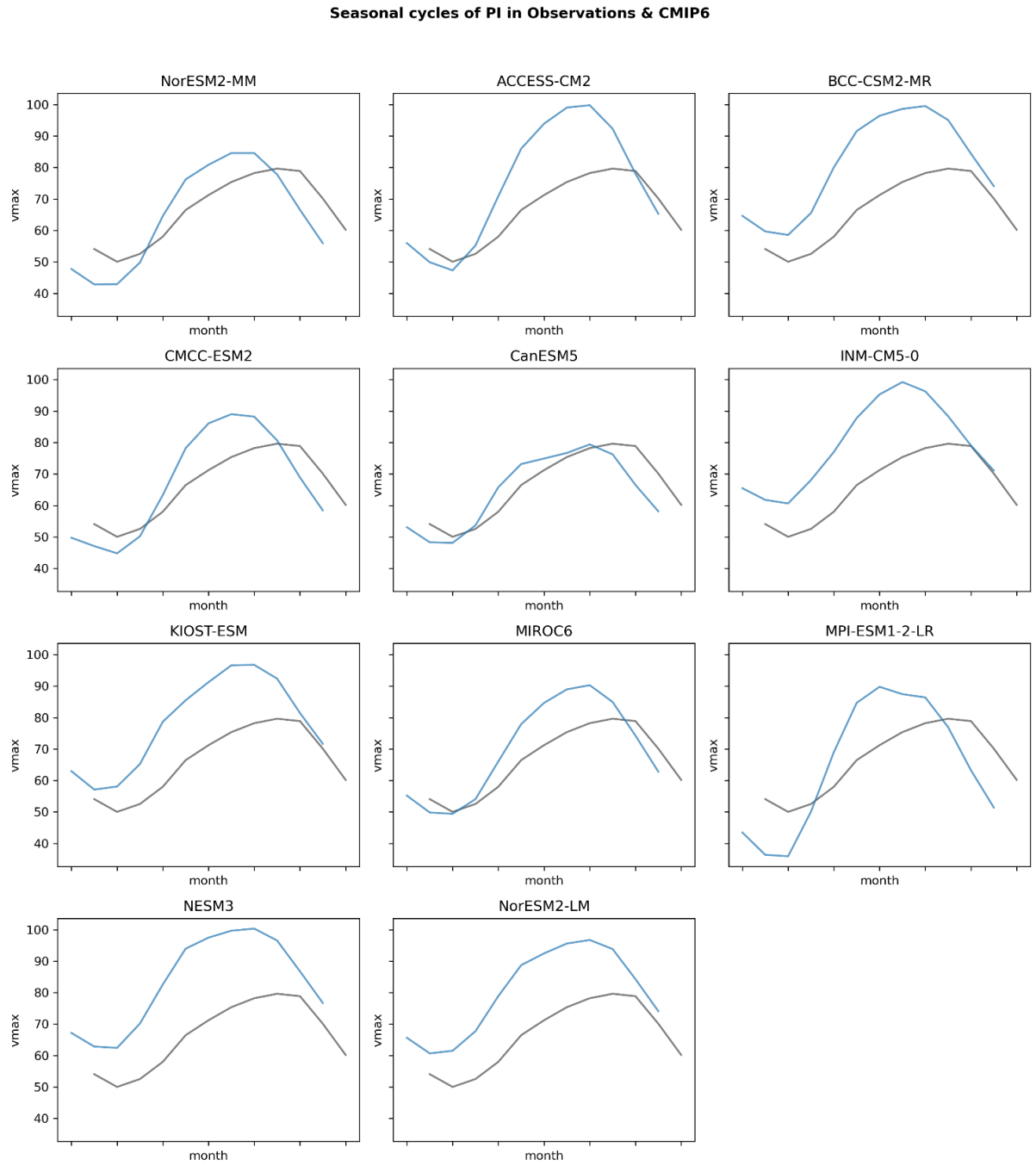

Figure A.8: *Seasonal cycles of potential intensity in observations (ERA5) and CMIP6.*